MAPK-induced miR-29 targets MAFG and suppresses melanoma progression

Olga Vera[1], Ilah Bok[1,2], Neel Jasani[1,2], Koji Nakamura[1], Xiaonan Xu[1], Nicol Mecozzi[1,3], Florian A. Karreth[1]*

[1] Department of Molecular Oncology, H. Lee Moffitt Cancer Center and Research Institute, Tampa, Florida, USA

[2] Cancer Biology PhD program, University of South Florida, Tampa, Florida, USA

[3] Department of Biology, University of Pisa, Pisa, Italy.

*Corresponding Author:

Florian A. Karreth

Email: florian.karreth@moffitt.org

Phone: 813-745-1851

KEYWORDS: melanoma, miR-29, MAPK pathway, MAFG.

ABSTRACT

The tumor suppressive miR-29 family of microRNAs is encoded by two clusters, miR-29b1~a and miR-29b2~c, and is regulated by several oncogenic and tumor suppressive stimuli. Here we investigated whether oncogenic MAPK hyperactivation regulates miR-29 abundance and how this signaling axis impacts melanoma development. Using mouse embryonic fibroblasts and human melanocytes, we found that oncogenic MAPK signaling stimulates p53-independent and p53-dependent transcription of pri-miR-29b1~a and pri-miR-29b2~c, respectively. Expression analyses revealed that while pri-miR-29a~b1 remains elevated, pri-miR-29b2~c levels decrease during melanoma progression. Using a rapid mouse modeling platform, we showed that inactivation of miR-29 in vivo accelerates the development of frank melanomas and decreases overall survival. We identified MAFG as a relevant miR-29 target that has oncogenic potential in melanocytes and is required for growth of melanoma cells. Our findings suggest that MAPK-driven miR-29 induction constitutes a tumor suppressive barrier by targeting MAFG, which is overcome by attenuation of miR-29b2~c expression.

INTRODUCTION

Malignant melanoma is an aggressive cancer that arises as a consequence of activation of proto-oncogenes, most commonly BRAF and NRAS. Despite the recent advances in melanoma therapy, most patients still succumb to the disease. A better understanding of the molecular biology of melanoma is needed to identify new therapeutic targets. Non-coding RNAs (ncRNAs) are critical regulators of cell biology whose alteration can lead to the development of cancer, including melanoma. ncRNAs can be classified based on their length into long non-coding RNAs (lncRNAs), those ncRNAs exceeding 200 nucleotides, and small non-coding RNAs, ranging from 18-200 nucleotides (Ponting et al. 2009; Djebali et al. 2012). MicroRNAs (miRNAs) are a group of small non-coding RNAs that repress gene expression by binding to 3'UTRs of target mRNAs (Davis and Hata 2009). To date, various miRNAs have been reported to regulate the biology of melanoma cells (reviewed in (Wozniak et al. 2016; Fattore et al. 2017; Romano and Kwong 2017)) including miR-29a, for which tumor suppressive potential was recently described in in vitro (Xiong et al. 2018).

The miR-29 family is encoded by two clusters, miR-29b1~a and miR-29b2~c, located on chromosomes 7q32.2 and 1q32.2 in humans, respectively (Kriegel et al. 2012; Alizadeh et al. 2019). Expression of the miR-29 clusters produces primary transcripts pri-miR-29b1~a and pri-miR-29b2~c, which are processed to generate three mature miRNAs, miR-29a, miR-29b, and miR-29c, that are highly conserved across species and share identical seed sequences (Kriegel et al. 2012). miR-29 is considered a tumor suppressor miRNA given its ability to repress genes involved in proliferation and cell survival such as AKT3 (Ugalde et al. 2011; Wei et al. 2013), DNMT3A/B (Nguyen et al. 2011), MCL1 (Mott et al. 2007), and CDK6 (Zhao et al. 2010). Over the last decade, miR-29 has

emerged as a major regulatory hub that integrates signaling from potent oncogenes and tumor suppressors. Indeed, miR-29 expression is repressed by the oncogenes c-Myc, Hedgehog, and NF-κB (Chang et al. 2008; Mott et al. 2010; Zhang et al. 2012b). NRF2 was reported to stimulate or suppress miR-29 expression in different cell types (Kurinna et al. 2014; Shah et al. 2015), and p53 promotes miR-29 expression when stimulated by aging or chronic DNA damage (Ugalde et al. 2011).

In this study we tested if oncogenic MAPK signaling represses the expression of the tumor suppressive miR-29 family similar to other oncogenic pathways. Surprisingly, we found that miR-29b1~a expression is enhanced directly by the MAPK pathway and remains elevated in melanoma. Conversely, MAPK signaling requires p53 to promote miR-29b2~c expression, which enables attenuation of miR-29b2~c upon melanoma progression. Inactivation of miR-29 in a melanoma mouse model augmented tumor development. Finally, we identified MAFG as a miR-29 target whose de-repression may be important for melanoma progression.

RESULTS

Oncogenic BRAF and KRAS increase the abundance of mature miR-29 in mouse embryonic fibroblasts

The expression of miR-29 is repressed by several oncogenes – c-Myc, Hedgehog, NF-κB, and, in certain contexts, NRF2 (Chang et al. 2008; Mott et al. 2010; Zhang et al. 2012b; Kurinna et al. 2014; Shah et al. 2015) – while the tumor suppressor p53 promotes miR-29 expression in response to ageing and DNA damage stress (Ugalde et al. 2011). We sought to examine if oncogenic BRAF and KRAS also lower miR-29 abundance. To this end, we ectopically expressed $Braf^{V600E}$ and $Kras^{G12D}$ in wildtype MEFs. Both oncogenes enhanced activation of the MAPK pathway, as indicated by an increase in phospho-ERK (Figure 1A). Unexpectedly, overexpression of $Braf^{V600E}$ or $Kras^{G12D}$ led to an increase of mature miR-29a, -29b, and -29c, an effect that was more pronounced in the $Braf^{V600E}$-expressing cells (Figure 1A). In MEFs, supraphysiological expression of $Kras^{G12D}$ enhances p53 activity compared to $Kras^{G12D}$ expressed at physiological levels (Tuveson et al. 2004), which could explain the increase in miR-29 levels. As physiological expression of $Braf^{V600E}$ and $Kras^{G12D}$ provokes limited p53 activation, we examined miR-29 expression in MEFs carrying Cre-inducible endogenous $Braf^{V600E}$ and $Kras^{G12D}$ alleles (LSL-$Braf^{V600E}$ and LSL-$Kras^{G12D}$) (Jackson et al. 2001; Perna et al. 2015). Adenoviral-Cre mediated activation of endogenous $Braf^{V600E}$ or $Kras^{G12D}$ induced the upregulation of miR-29a, -29b, and -29c (Figure 1B and Supplementary Figure 1A), indicating that physiological expression of these oncogenes also enhances the expression of the miR-29 family.

To determine if the regulation of miR-29 occurs at the transcriptional level, we assessed the expression of the miR-29b1~a and miR-29b2~c clusters using qPCR TaqMan probes

to detect the primary miRNA transcripts, pri-miR-29b1~a and pri-miR-29b2~c. Ectopic overexpression of oncogenic $Braf^{V600E}$ or $Kras^{G12D}$ increased both pri-miR-29b1~a and pri-miR-29b2~c (Figure 1C). Similarly, endogenous activation of $Braf^{V600E}$ or $Kras^{G12D}$ resulted in upregulation of both pri-miR-29b1~a and pri-miR-29b2~c (Figure 1D and Supplementary Figure 1B), indicating that oncogenic BRAF and KRAS indeed promote the transcription of both miR-29 clusters. MiR-29 may function as a melanoma tumor suppressor (Xiong et al. 2018) and the $BRAF^{V600E}$ mutation is found in over 50% of melanoma cases (Davies et al. 2002; Ascierto et al. 2012). We therefore focused our further analyses on the regulation of miR-29 by oncogenic BRAF.

pri-miR-29b1~a and pri-miR-29b2~c are transcribed via the MAPK pathway and p53

To further assess if p53 plays a role in the regulation of miR-29 by oncogenic BRAF, we first ascertained that DNA damage-induced p53 activation enhances the expression of miR-29 in MEFs, as measured by mature miRNA qRT-PCR (Supplementary Figure 1C and 1D). We also tested if DNA damage increased miR-29 transcription and, surprisingly, found that Doxorubicin and Mitomycin C induced only the transcription of pri-miR-29b2~c (Figure 2A). This is at odds with the results obtained by mature miRNA qRT-PCRs where p53 activation increased expression of all three miR-29 family members. It is possible that the mature miR-29 qRT-PCR approach is unable to distinguish between miR-29a and miR-29c, which only differ in one nucleotide, as has been suggested previously (Kurinna et al. 2014). Indeed, miR-29a and miR-29c Taqman assays were unable to distinguish between miR-29a and miR-29c mimics transfected into A375 melanoma cells (Supplementary Figure 1E). Thus, the increased abundance of mature

miR-29a upon DNA damage is most likely explained by elevated transcription of the highly homologous miR-29c family member.

The lack of pri-miR-29b1~a transcription upon p53 activation suggests that oncogenic Braf^{V600E}-induced pri-miR-29b1~a expression is independent of p53. To further analyze the role of p53 in regulating Braf^{V600E}-induced transcription of pri-miR-29b1~a and pri-miR-29b2~c we silenced p53 with a retroviral shRNA in LSL-Braf^{V600E} MEFs (Supplementary Figure 1F). Retroviral infection did not interfere with Braf^{V600E}-induced pri-29b1~a and pri-miR-29b2~c expression (Supplementary Figure 1G). As expected, induction of Braf^{V600E} by adenoviral Cre failed to increase pri-miR-29b2~c expression in the absence of p53 (Figure 2B). By contrast, Braf^{V600E} increased pri-miR-29b1~a expression in p53-silenced MEFs to the same extent as in p53-proficient MEFs (Figure 2B), indicating that Braf^{V600E}-mediated regulation of pri-miR-29b1~a in MEFs is indeed independent of p53. To test the physiological consequence of Braf^{V600E}-induced pri-miR-29b1~a expression, we performed a miR-29 Luciferase reporter assay in p53-silenced LSL-Braf^{V600E} MEFs. Induction of Braf^{V600E} decreased Luciferase activity, suggesting that the extent of miR-29b1~a upregulation is sufficient for target repression (Figure 2C).

Given that Braf^{V600E}-induced miR-29b1~a expression is independent of p53, we examined the involvement of the MAPK pathway downstream of oncogenic BRAF in miR-29 regulation. To this end, we treated LSL-Braf^{V600E} MEFs with the MEK inhibitor AZD6244 (Selumetinib) with or without induction of Braf^{V600E}. 24 hours of AZD6244 treatment decreased basal and Braf^{V600E}-induced MAPK pathway activity, as shown by reduced levels of pErk and the downstream transcriptional target c-Jun (Figure 2D and 2E). MEK inhibition also decreased basal and Braf^{V600E}-induced pri-miR-29b1~a expression (Figure 2D). This effect was also observed in p53-silenced LSL-Braf^{V600E}

MEFs (Figure 2E), indicating that oncogenic BRAF regulates miR-29b1~a independently of p53 via the MAPK pathway. AZD6244 treatment blunted Braf^{V600E}-induced pri-miR-29b2~c expression, possibly due to reduced p53 expression (Figure 2D). Neither Braf^{V600E} expression nor MEK inhibition affected pri-miR-29b2~c levels in the absence of p53 (Figure 2E). These data suggest differential regulation of the miR-29 clusters by Braf^{V600E} in MEFs: while miR-29b1~a is controlled by the MAPK pathway, miR-29b2~c expression depends on p53.

The MAPK pathway regulates miR-29 expression in human melanocytes and melanoma cells

We next examined if the regulation of miR-29 observed in MEFs is conserved in human melanocytes and melanoma cell lines. Treatment of the immortalized human melanocyte lines Hermes1 and Hermes3A with Doxorubicin increased p53 and p21 (Figure 3A). This induction of p53 robustly elevated pri-miR-29b2~c levels (Figure 3A), indicating that p53 regulates pri-miR-29b2~c also in melanocytes. To analyze miR-29 regulation by the MAPK pathway in melanocytes we starved Hermes1 and Hermes3A cells of TPA, a phorbol ester that stimulates the MAPK pathway and that is required for melanocyte proliferation in vitro. Re-stimulation with TPA increased pERK levels and pri-miR-29b1~a expression (Figure 3B). Interestingly, TPA also moderately enhanced pri-miR-29b2~c expression (Figure 3B). Further, MEK inhibition with AZD6244 in Hermes1 and Hermes3A cells cultured in the presence of TPA diminished the expression of pri-miR-29b1~a and pri-miR-29b2~c (Figure 3C). Moreover, AZD6244 also decreased the levels of pri-miR-29b1~a and pri-miR-29b2~c in A375 and WM164 human melanoma cell lines (Figure 3D). Thus, while p53 potently stimulates miR-

29b2~c in both MEFs and melanocytes, the MAPK pathway induces expression of both miR-29 clusters in cells of the melanocytic lineage.

Our results indicate that Braf^{V600E}-induced expression of miR-29 may form a tumor suppressive barrier that restricts the full transformation of melanocytes. Thus, to analyze pri-miR-29 expression during melanomagenesis we performed RNA sequencing on four wildtype BRAF human melanocyte cell lines (Hermes1, Hermes2, Hermes3A, and Hermes4B) and five human melanoma cell lines (WM35, 1205Lu, WM164, SKMel28 and WM793) harboring the oncogenic BRAF^{V600E} mutation. In addition, we interrogated pri-miR-29 expression in a publicly available RNAseq dataset (Kunz et al. 2018) containing 23 nevi and 57 primary melanomas. In agreement with our observations, we found that there was a trend towards increased pri-miR-29b1~a expression in melanoma cell lines and primary melanomas compared to melanocyte cell lines and nevi, respectively (Figure 3E and 3F). Notably, expression of pri-miR-29b2~c was attenuated in melanoma cell lines and primary melanomas (Figure 3E and 3F), suggesting that a reduction of miR-29b and/or miR-29c is associated with melanoma progression.

To further analyze miR-29 regulation during melanocyte transformation, we examined the consequences of chronic BRAF^{V600E} expression in human melanocytes. We delivered lentiviral HA-tagged BRAF^{V600E} to Hermes1 and Hermes3A cells, which resulted in the emergence of four independent clones, one from Hermes1 (H1B) and three from Hermes3A (H3B2, H3B4 and H3B8). These cell lines are morphologically different from the parental lines, express ectopic BRAF^{V600E}, and exhibit increased MAPK signaling as shown by elevated pERK and c-Jun (Supplementary Figure 2A and 2B), which enables these cells to proliferate in the absence of TPA (Supplementary Figure 2C and 2D).

Notably, all four cell lines lost expression of p53 (Supplementary Figure 2A and 2B), and RNA sequencing revealed that similar to melanoma cell lines and primary melanomas, H1B cells exhibited reduced pri-miR-29b2~c expression and a trend towards increased pri-miR-29b1~a levels (Figure 3G). Finally, expression of both pri-miR-29b1~a and pri-miR-29b2~c was sensitive to AZD6244 treatment in H1B and H3B8 cells (Figure 3H). These observations indicate that while MAPK signaling enhances transcription of miR-29b1~a in melanocytes, miR-29b2~c is regulated by the MAPK pathway and p53. Furthermore, melanoma progression is associated with decreased pri-miR-29b2~c levels, possibly through impaired p53 activity.

miR-29 inactivation promotes melanoma progression

To examine the role of miR-29 in melanoma formation in vivo, we first tested a miRNA sponge approach to inactivate miR-29 in vitro. To this end, we either transfected A375 melanoma cells with a hairpin inhibitor of miR-29a, which is upregulated in melanoma cells (Figure 3E), or delivered a lentiviral bulged miR-29 sponge construct. While inhibition of miR-29 enhanced only the focus formation capacity of A375 cells (Figure 4A), the miR-29 sponge construct increased proliferation and focus formation (Figure 4B and 4C). In addition, the miR-29 sponge increased the activity of a miR-29 Luciferase reporter (Figure 4D), indicating that this approach could be used in combination with our rapid melanoma mouse modeling platform (Bok et al. 2019) to assess continuous miR-29 inactivation in vivo. Embryonic stem cell (ESC)-derived chimeras produced by this approach are topically treated with 4OH-Tamoxifen (4-OHT) to activate melanocyte-specific Cre, which induces $Braf^{V600E}$ expression and heterozygous Pten deletion (Figure 4E), thereby initiating melanomagenesis. Cre also induces reverse transactivator (rtTA3) expression, enabling melanocyte-specific expression of

transgenes upon Doxycycline administration (Figure 4E). We targeted ESCs with a Doxycycline (Dox)-inducible, GFP-linked miR-29 sponge allele or GFP as a control and produced miR-29 sponge and GFP control chimeras having similar ESC contribution. Notably, chimeras expressing the miR-29 sponge developed melanoma faster (Figure 4F) and exhibited reduced overall survival (Figure 4G), indicating that inactivation of miR-29 accelerates melanoma development.

Melanoma cells are addicted to high levels of miR-29 target genes

We derived a melanoma cell line from a miR-29 sponge chimera to validate the functionality of the miR-29 sponge in mice and to examine the effects of restoring miR-29 activity. Withdrawing Dox from the melanoma cell line turned off miR-29 sponge expression and enhanced repression of a miR-29 Luciferase reporter (Figure 5A), confirming that the sponge inactivated endogenous miR-29. Moreover, Dox withdrawal reduced proliferation (Figure 5B) and colony formation (Figure 5C) of the miR-29 sponge melanoma cells, indicating that continued miR-29 inactivation, and thus miR-29 target overexpression, is required to maintain the transformed state.

miR-29 may elicit its tumor suppressive potential by repressing targets such as AKT3, DNMT3A/B, or MCL1 (Mott et al. 2007; Nguyen et al. 2011; Ugalde et al. 2011; Wei et al. 2013); however, miR-29 hairpin inhibitors failed to increase the expression of these validated targets in A375 melanoma cells (Supplementary Figure 3A). Thus, alternative miR-29 targets must be responsible for the effect of miR-29 hairpins on A375 focus formation (Figure 4A). To identify miR-29 targets with relevance to melanoma progression, we transfected A375 cells with miR-29a mimics and performed RNA sequencing. Genes that were reduced in response to miR-29a mimics were further

prioritized based on three criteria: 1) the presence of predicted high-confidence miR-29 binding sites, 2) increased expression in primary melanoma compared to nevi in the GSE112509 dataset, and 3) a negative correlation in expression with pri-miR-29b2~c in the GSE112509 dataset (Supplementary Figure 3B). This analysis yielded 9 candidate target genes: KCTD5, MYBL2, SLC31A1, MAFG, RCC2, TUBB2A, SH3BP5L, SMS, and NCKAP5L (Figure 5D and 5E and Supplementary Figure 3C and 3D). Notably, high expression of these 9 putative miR-29 targets is associated with poorer survival of melanoma patients (Figure 5F), implicating these miR-29 targets in melanoma progression.

The miR-29 target MAFG promotes the transformed state in melanoma

The finding that miR-29 restoration impairs melanoma cell growth (Figure 5B and 5C) suggests that the identified miR-29 targets could have oncogenic potential in melanoma. We selected MAFG (Figure 5D and 5E) for this further analysis because MAFG has been implicated in melanoma as an epigenetic regulator and transcriptional repressor (Fang et al. 2016). In addition, phosphorylation by ERK promotes MAFG protein stability (Fang et al. 2016), suggesting that hyperactive MAPK signaling could increase MAFG levels in melanoma. To first validate MAFG as a target of miR-29 we transfected miR-29a, miR-29b, or miR-29c mimics into $BRAF^{V600E}$-expressing melanocytes (H1B), and melanoma cells (WM164). We observed a general reduction of MAFG mRNA and protein expression (Figure 6A and 6B). By contrast, hairpin inhibitors of miR-29a, miR-29b, or miR-29c increased MAFG mRNA and protein levels in these cell lines (Figure 6A and 6B). Next, we created a MAFG 3'UTR Luciferase reporter and mutated the seed sequence of the miR-29 binding site with the highest prediction score (Supplementary Figure 4A).

Co-transfection of miR-29 inhibitor with the wildtype MAFG 3'UTR reporter into H1B, H3B8, A375, and WM164 cells increased Luciferase activity (Figure 6C and Supplementary Figure 4B). By contrast, miR-29 mimics reduced the activity of the wildtype MAFG 3'UTR reporter and this effect was partially rescued by the miR-29 binding site mutation (Figure 6D and Supplementary Figure 4C). These findings indicate that MAFG is a bona fide target of miR-29.

We next assessed whether MAFG plays a role in melanoma development. First, we analyzed MAFG expression in melanocytes and melanoma cell lines and found that MAFG mRNA levels are increased in melanoma cell lines (Figure 6E). This finding corroborates the increase in MAFG mRNA observed in primary melanomas compared to nevi (Figure 5E). MAFG protein expression was similarly elevated in melanoma cell lines compared to melanocytes (Figure 6F and 6G). TPA treatment increased MAFG protein expression in Hermes1 and Hermes3A cells (Figure 6H), which can be attributed to ERK-mediated MAFG stability (Fang et al. 2016). Interestingly, MAFG protein levels are further increased in $BRAF^{V600E}$-expressing Hermes cells in which p53 is lost and pri-miR-29b2~c is reduced (Figure 6H), suggesting gradual MAFG elevation during melanoma progression. Next, we examined the effects of modulating MAFG expression on melanocytes and melanoma cells. Stable overexpression of lentiviral MAFG in Hermes1 melanocytes increased proliferation (Figure 7A) and conferred the ability to form colonies (Figure 7B). Conversely, silencing of MAFG in A375 and WM164 melanoma cells with a siRNA pool to reduce off-target effects markedly attenuated proliferation (Figure 7C and 7E) and colony formation (Figure 7D and 7F), indicating that MAFG has oncogenic potential and is required for the growth of melanoma cells.

DISCUSSION

Deregulation of miRNAs frequently occurs in cancer and is thought to play critical roles in all aspects of tumorigenesis. Here, we investigated the deregulation of miR-29, a miRNA with tumor suppressive properties in various cancer types (reviewed in (Alizadeh et al. 2019)), in melanoma progression. Using MEFs and human melanocytes, we uncovered paradoxical upregulation of miR-29 downstream of oncogenic RAS and BRAF via MAPK signaling and p53. Diminished expression of the p53-dependent miR-29b2~c cluster is associated with melanoma progression and inactivation of miR-29 promotes melanoma development in mice. De-repression of MAFG, which we identified as a bona fide target of miR-29, may contribute to melanoma progression.

Previous studies have shown that p53 regulates the expression of both miR-29b1~a and miR-29b2~c (Ugalde et al. 2011; Chen et al. 2018). However, our results indicate that transcription of miR-29b1~a is independent of p53, both in MEFs and in melanocytes. Rather, miR-29b1~a is regulated directly via MAPK signaling. This discrepancy is likely due to the fact that mature miR-29 species were analyzed by qRT-PCR in the previous studies, a method that failed to distinguish mature miR-29 family members, as has been suggested previously (Kurinna et al. 2014). Several studies have shown cluster-specific regulation of miR-29: NRF2 regulates miR-29b1~a in keratinocytes (Kurinna et al. 2014) and Gli and NF-κB promote miR-29b1~a expression in cholangiocarcinoma cells (Mott et al. 2010), while Myc represses expression of both miR-29b1~a and miR-29b2~c in B-cell lymphoma (Chang et al. 2008; Zhang et al. 2012a). Thus, each of the two miR-29 clusters is regulated by a distinct repertoire of cancer–associated pathways. Further studies into the regulation of miR-29 ought to include measurements of the

primary miR-29 transcripts to avoid ambiguous results stemming from detecting mature miR-29 with low-specificity qRT-PCR methods.

Interestingly, while MAPK signaling promotes expression of only miR-29b1~a in MEFs, the MAPK pathway induces transcription of both clusters in human melanocytes. It is possible that the regulation of miR-29b2~c is not conserved between mouse and human or that miR-29b2~c expression is controlled in a cell type-specific manner. Moreover, the induction miR-29b2~c by MAPK signaling in melanocytes was much more modest than by p53 activation. It remains to be investigated how MAPK signaling and p53 activation coordinately enhance miR-29b2~c expression upon acquisition of an oncogenic BRAF mutation. p53 may be induced by oncogene-activated MAPK pathway hyperactivation as ERK has been reported to phosphorylate p53 at serine 15 (Wu 2004). Moreover, MAPK activation increases expression of Cyclin D, which releases E2F-1 via RB phosphorylation, thereby promoting p14ARF transcription (Peeper et al. 1997; Bates et al. 1998). p14ARF in turn stabilizes p53 through inhibition of MDM2 (Sherr and Weber 2000). MAPK hyperactivation downstream of oncogenic BRAF is a critical driver of melanoma development (Davies et al. 2002), and p53 activation in response to mutant BRAF has been observed in melanocytes (Yu et al. 2009; Ko et al. 2019). Thus, oncogenic BRAF may activate p53 in melanocytes via the MAPK pathway, which in turn induces pri-miR-29b2~c expression. Alternatively, MAPK signaling may directly promote pri-miR-29b2~c expression, and p53 serves as a critical permissive factor that is required for pri-miR-29b2~c transcription. Oncogenic BRAF only very moderately activates p53 (Lloyd et al. 1997; Sheu et al. 2012), suggesting that BRAF may indeed work in concert with rather than through p53.

Numerous reports describe tumor suppressive functions of miR-29 in cultured cells, including in melanoma cell lines (Nguyen et al. 2011; Yu et al. 2014; Cui et al. 2015; Nishikawa et al. 2015; Chen et al. 2018; Xiong et al. 2018), which we corroborated in our study. Given the tumor suppressive functions of miR-29 and its regulation by MAPK signaling, we hypothesized that MAPK hyperactivation could provoke a miR-29-dependent barrier that prevents melanoma formation. The MAPK pathway is almost universally hyperactivated in melanoma, owing to the frequent activating mutations in BRAF and NRAS (Davies et al. 2002; Satyamoorthy et al. 2003; Gray-Schopfer et al. 2005; Sumimoto et al. 2006). Notably, growth arrested nevi are common in humans and >80% of nevi harbor $BRAF^{V600E}$ mutations (Wu et al. 2007; Yeh et al. 2013), suggesting that such a barrier indeed exists (Michaloglou et al. 2005). To overcome this barrier, BRAF/NRAS mutant melanocytes must reverse the increase in miR-29 levels. We observed that miR-29b2~c expression is decreased in i) melanocytes upon chronic expression of $BRAF^{V600E}$, which also provoked loss of p53, ii) melanoma cell lines compared to melanocytes, and iii) primary melanomas compared to nevi. It is tempting to speculate that while miR-29b1~a remains elevated due to continuous MAPK hyperactivation, impaired p53 activity leads to decreased miR-29b2~c expression, thereby promoting melanoma progression. p53 may play a role in the growth arrest of nevi (Gray-Schopfer et al. 2006; Yu et al. 2009; Terzian et al. 2010), and p53 inactivation in genetically engineered mice promotes melanoma development in the context of $BRAF^{V600E}$ (Viros et al. 2014). Moreover, p53 mutations and copy number losses occur frequently in cutaneous melanoma (Berger et al. 2012; Hodis et al. 2012; Krauthammer et al. 2012; Krauthammer et al. 2015; Zhang et al. 2016). Even more common are deletions of CDKN2A (Hodis et al. 2012; Krauthammer et al. 2012; Krauthammer et al. 2015; Zhang et al. 2016), which besides p16INK4A encodes ARF, a positive regulator of

p53 protein stability. A p16INK4A-independent role for ARF in melanoma suppression has been described (Hewitt et al. 2002; Sharpless et al. 2003; Freedberg et al. 2008). Additionally, a subset of melanomas harbor amplifications of MDM2 (Muthusamy et al. 2006; Cancer Genome Atlas 2015), an E3 ubiquitin ligase that promotes the turnover of p53. Thus, multiple mechanisms of p53 inactivation occur in melanoma, all of which could lead to a reduction in miR-29b2~c expression.

Using a high-throughput mouse modeling approach, we inactivated miR-29 through expression of a sponge construct specifically in $Braf^{V600E}$; $Pten^{\Delta/+}$ melanocytes. In agreement with our hypothesis, miR-29 inactivation accelerated the development of melanoma. Not only is this the first model used to study miR-29 inactivation in tumorigenesis, our approach also affirms that synthetic miRNA sponges are powerful tools to examine miRNA function in vivo. One advantage over traditional modeling approaches, such as the previously published conditional knock-out allele of miR-29b1~a (Kogure et al. 2012), is that a miRNA sponge has the potential to inactivate all members of a miRNA family. However, it is usually not clear how well a sponge interacts with each family member, especially in cases like the miR-29 family where one member, miR-29b, also localizes to the nucleus (Hwang et al. 2007). Thus, future studies using alternative approaches such as CRISPR/Cas9-mediated specific deletion of individual clusters or miRNAs will further elucidate the role of each miR-29 family member in melanoma. This will also address if a decrease in miR-29b2~c in melanoma simply lowers the overall miR-29 levels to promote melanoma, indicative of functional redundancy of miR-29a, -29b, and -29c, or if miR-29b and/or miR-29c have specific functions that are impaired upon miR-29b2~c downregulation.

Since we did not observe changes in the expression of the validated miR-29 targets AKT3, MCL1, and DNMT3B, we identified new targets that might constitute vulnerabilities of melanoma. Of the 9 genes identified by our approach (KCTD5, MYBL2, SLC31A1, MAFG, RCC2, TUBB2A, SH3BP5L, SMS and NCKAP5L), RCC2, MYBL2 and SLC31A1 have previously been identified as miR-29 targets (Martinez et al. 2011; Matsuo et al. 2013; Wu et al. 2013; Hu et al. 2014; Sun et al. 2018). We selected MAFG for further analyses because the protein is stabilized by ERK-mediated phosphorylation (Fang et al. 2016), suggesting that MAPK signaling converges on MAFG via ERK and miR-29. In addition to being repressed by miR-29, TCGA data indicate copy number gains of MAFG in melanoma. Thus, MAFG is deregulated in melanoma through multiple mechanisms, and our in vitro data further suggest that MAFG plays an important role in melanoma progression and maintenance. Oncogenic roles for MAFG have so far been described in lung, ovarian, colorectal, and liver cancer (Fang et al. 2016; Vera et al. 2017; Liu et al. 2018), and, interestingly, MAFG is a binding partner of CNC and BACH protein families, including NRF2 (reviewed in (Katsuoka and Yamamoto 2016)). NRF2 is a critical regulator of redox biology and cellular metabolism (Hirotsu et al. 2012; Hayes and Dinkova-Kostova 2014), and mutations in NRF2 and its negative regulator KEAP1 occur frequently in lung and upper airway cancers (Cloer et al. 2019). By contrast, mutations in NRF2/KEAP1 are rarely observed in melanoma. Future studies will address if MAFG's functions in melanoma require binding to and enhancing of the transcriptional activity of NRF2, or if other binding partners are critical. Thus, our work has uncovered that miR-29 prevents melanoma progression downstream of MAPK signaling by repressing MAFG.

MATERIALS AND METHODS

Cell culture and treatments

The human immortalized melanocytes cell lines Hermes1, Hermes2, Hermes3A and Hermes4B were obtained from the Functional Genomics Cell Bank at St George's, University of London, UK, and cultured in RPMI media supplemented with 10% FBS, 10ng/mL hSCF (R&D, Cat # 255-SC), 200nM TPA (Sigma, Cat # P8139), 200pM Cholera Toxin (Sigma, Cat # C8052), and 10nM Endothelin-1 (Sigma, Cat # E7764) at 37˚C in a humidified atmosphere containing 10% CO_2. A375 cells were purchased from ATCC and WM164 cells were a gift from M. Herlyn. Both cell lines were cultured in RPMI containing 5% FBS at 37˚C in a humidified atmosphere containing 5% CO_2. $BRAF^{V600E}$-expressing human melanocytes cell lines were derived by infecting Hermes1 and Hermes3A with a $BRAF^{V600E}$ lentivirus (provided by L. Wan) for six hours in the presence of 8μg/mL Polybrene. Transduced cells were selected in 100nM of Hygromycin (Invivogen, Cat # ant-hg-1) for seven days in the absence of TPA. Four independent clones were picked and expanded until stable cell lines were obtained. MEFs were generated from E13.5-E14.5 embryos from LSL-$Braf^{V600E}$ (Karreth et al., Mol Cell 2009) or LSL-$Kras^{G12D}$ mice (Jackson et al., Genes & Dev, 2001) and cultured in DMEM containing 10% FBS at 37˚C in a humidified atmosphere containing 5% CO_2. Wildtype males were derived from littermate embryos that did not harbor the LSL-$Braf^{V600E}$ or LSL-$Kras^{G12D}$ alleles. To recombine floxed alleles, MEFs were infected with approximately 10^7pfu/mL Ad5CMVCre or Ad5CMVempty adenovirus obtained from the University of Iowa Viral Vector Core. Lenti-X 293T cells were obtained from Takara and cultured in DMEM containing 10% FBS at 37˚C in a humidified atmosphere containing 5% CO_2. All cells were routinely tested for mycoplasma using MycoAlert Plus (Lonza,

Cat # LT07-710), and human melanoma cell lines were STR authenticated by Moffitt's Molecular Genomics Core. Doxorubicin (Fisher Scientific, Cat # BP25131) was used at a final concentration of 10μM for 24 hours and AZD6244 (Selleckchem, Cat # S1008) was used at a final concentration of 0.5μM for 8 or 24 hours.

RNA isolation, RNAseq and quantitative RT-PCR

Total RNA was isolated using TRI-Reagent (Zymo Research, Cat # R2050-1-200) and mature miRNAs were isolated using the miRNeasy Mini Kit (Qiagen, Cat # 217004) according to the manufacturers' recommendations. For qRT-PCR, 500ng of total RNA were retrotranscribed using PrimeScript RT Master Mix (Takara Bio, Cat. # RR036A), and subsequent TaqMan assay-based or SYBR Green-based qPCR were performed using PerfeCTa qPCR ToughMix (QuantaBio, Cat. # 97065-960) or PerfeCTa SYBR Green FastMix (QuantaBio, Cat. # 95073-012), respectively. Mature miRNAs were retrotranscribed using TaqMan MicroRNA Reverse Transcription Kit (Thermo Fisher, Cat # 4366596) and analyzed by qPCR using PerfeCTa qPCR ToughMix (QuantaBio, Cat. # 97065-960). Samples were analyzed in triplicate using the StepOne Plus PCR system (Applied Biosystems, USA). The comparative threshold cycle method ($2^{-\Delta\Delta Ct}$) was used to calculate the relative expression levels. snoU6 was used as endogenous control for mature miRNAs while GAPDH or β-actin were used for mRNAs and pri-miRNAs. TaqMan Probes for expression analyses were purchased from Thermo Fisher Scientific (U6 snRNA: 001973; mouse β-actin: Mm02619580_g1; human β-ACTIN: mouse Cdkn1a: Mm04205640_g1; mmu-mir-29a: Mm03306859_pri; mmu-mir-29b-2: Mm03307196_pri; mmu-mir-29c: Mm03306860; mmu-mir-29b-1; Mm03306189_pri; hsa-mir-29a: Hs03302672_pri; hsa-mir-29c: Hs04225365_pri; hsa-miR-29a: 002112; hsa-miR-29b: 000413; hsa-miR-29c: 000587). Primers for SYBR Green qPCR were

designed to target MAFG (Forward: 5'-CACCCTTCTCTCTTCCCTGCAA-3'; Reverse: 5'-TCTCTCTCCCGCAACTCTCTCT-3'), DNMT3B (Forward: 5'-AGTCGAAGGTGCGTCGTG-3'; Reverse: 5'-AGCCATTGTTCTCGGCTCT-3). AKT3 (Forward: 5'-GAGGACCGCACACGTTTCTA-3'; Reverse: 5'-TGTCTTCATGGTGGCTGCAT-3), MCL1 (Forward: 5'-GAGGACGAGTTGTACCGGCAG-3'; Reverse: 5'-CGTTTTTGATGTCCAGTTTCCGA-3) and GAPDH (Forward: 5'-GAGAGACCCTCACTGCTG-3'; Reverse: 5'-GATGGTACATGACAAGGTGC-3').

RNA-sequencing

Total RNA from cells was isolated using RNA isolation kit (Qiagen) and analyzed for RIN. *Sequencing by the Biostatistics and Bioinformatics Core at Moffitt*: Double-stranded cDNA synthesis and library construction were performed using the Nugen Ovation Human RNA-seq library system (Nugen, San Carlos, CA). An Illumina NextSeq 550 instrument was used to generate 75 base pair paired-end RNA-seq reads. The raw reads were first assessed for quality using FastQC (http://www.bioinformatics.babraham.ac.uk/projects/fastqc/) and then trimmed by cutadapt (Martin 2011) (version 1.8.1) to remove reads with adaptor contaminants and low-quality bases. Read pairs with either end too short (<25bps) were discarded from further analysis. Trimmed and filtered reads were aligned to the GRCh37 human reference genome using STAR (Dobin et al. 2013) (version 2.5.3a). Uniquely mapped reads were counted by htseq-count (Anders et al. 2015) (version 0.6.1) using Gencode v25 primary annotation. Differential expression analysis was performed using DESeq2 taking into account of RNA composition bias (Love et al. 2014). Genes with fold-change>2 and false discovery rate (FDR) q-values< 0.05 were considered differentially expressed.

Sequencing by Novogene (Sacramento, CA). Library preparation was performed by NEBNext® Ultra™ RNA Library Prep Kit for Illumina® which is for non-stranded libraries. Sequencing was performed on the NovaSeq 6000 with a paired end 150 BP method. Downstream analysis was performed using a combination of programs including STAR, HTseq, Cufflink and our wrapped scripts. Alignments were parsed using Tophat program and differential expressions were determined through DESeq2/edgeR. GO and KEGG enrichment were implemented by the ClusterProfiler. Gene fusion and difference of alternative splicing event were detected by Star-fusion and rMATS software. Reference genome and gene model annotation files were downloaded from genome website browser (NCBI/UCSC/Ensembl) directly. Indexes of the reference genome was built using STAR and paired-end clean reads were aligned to the reference genome using STAR (v2.5). STAR used the method of Maximal Mappable Prefix(MMP) which can generate a precise mapping result for junction reads. HTSeq v0.6.1 was used to count the read numbers mapped of each gene. And then FPKM of each gene was calculated based on the length of the gene and reads count mapped to this gene. FPKM, Reads Per Kilobase of exon model per Million mapped reads, considers the effect of sequencing depth and gene length for the reads count at the same time, and is currently the most commonly used method for estimating gene expression levels (Mortazavi et al. 2008). Differential expression analysis between was performed using the DESeq2 R package (2_1.6.3). DESeq2 provide statistical routines for determining differential expression in digital gene expression data using a model based on the negative binomial distribution. The resulting P-values were adjusted using the Benjamini and Hochberg's approach for controlling the False Discovery Rate (FDR). Genes with an adjusted P-value < 0.05 found by DESeq2 were assigned as differentially expressed.

Plasmids

pBabe, pBabe-Braf^{V600E}, and pBabe-Kras^{G12D} were gifts from D. Tuveson. pLenti-GFP-puro was purchased from Addgene (plasmid #17448). The CMV promoter and puromycin in pLenti-GFP-puro were replaced with the EF1α promoter and blasticidin, respectively, using standard In-Fusion cloning (Takara Bio, Cat. # 638911) to create pLEGB. The Myc-DDK-tagged ORF clone of MAFG (RC221486, OriGene USA) was a gift from I. Ibanez de Caceres and cloned into pLEGB to replace GFP by In-Fusion cloning using the following primers Forward: 5'-acagtctagaggatcctcgactggatccggtacc-3'; Reverse: 5'-gaggttgattgtcgacttgggcatggccaggtagc-3'. The full length MAFG 3'UTR sequence (NM_002359.3 OriGene, USA) was a gift from I. Ibanez de Caceres and cloned into psiCHECK2 plasmid by In-Fusion cloning using the following primers Forward: 5'-taggcgatcgctcgagcgatcgccaaagtccaag-3'; Reverse: 5'-tgtatatgatcagcggaccgggccgctggccgcaa-3'. The psiCHECK2-miR29 Luciferase reporter was created by oligo cloning into psiCHECK2 using the following oligos: sense 5'-tcgacTAACCGATTTCAcGATGGTGCTAgc-3', antisense 5'-ggccgc TAGCACCATCgTGAAATCGGTTAg-3'.

Site-directed mutagenesis

We used the psiCHECK2-MAFG-3'-UTR to generate the miR-29 binding site mutant. Four different miR-29 binding sites were predicted by TargetScan, one of which is highly conserved. Site-directed mutagenesis was performed using the Q5 Site-Directed Mutagenesis Kit (NEB, Cat. # E0554S) according to the manufacturer's instructions. The primers designed to introduce mutations were: Forward-5'-gactctggtgaCCTTTGACCTGTGGGTGTC-3'; Reverse-5'-gaccgcactttaCCGCTGCACAAAACCTCA-3'.

Cell Transfection and lentiviral transduction

For miR-29 overexpression and inhibition, 100,000 cells/well were plated in 6-well plates and transfected with 150 or 50 nM of Dharmacon miRIDIAN microRNA miR-29a mimic (C-310521-07-0002), hairpin inhibitor (IH-310521-08-0002) or negative controls (CN-002000-01-05; IN-001005-01-05) using JetPrime (VWR Cat # 89129-924) according to the manufacturer's protocol and assayed after 48 hours. For Luciferase assays, cells were plated in 96-well plates at a density of 10,000 cells/well. psiCHECK2-MAFG-3'-UTR_wildtype or psiCHECK2-MAFG-3'UTR_miR-29-mutant were co-transfected with miR-29 mimics or inhibitors, following the procedure described above. Luminescence was assayed after 24 hours using the Dual Luciferase Assay System (Promega, Cat # E1960), according to the manufacturer's instructions. Similarly, miR-29-sponge melanoma cell lines were plated at a density of 10,000 cells/well and transfected with psiCHECK2 or psiCHECK2-miR-29 reporter following the same procedure. Luminescence was assayed after 48 hours using the Dual Luciferase Assay System. Results were normalized to the Renilla luminescence. For retroviral transductions, Lenti-X 293T cells were transfected with the retroviral vector and Eco helper plasmid at a 2:1 ratio. For lentiviral transductions, Lenti-X 293T cells were transfected with the lentiviral vector and the Δ8.2 and pMD2-VSV-G helper plasmids at a 9:8:1 ratio. Supernatants were collected 48 hours after transfection and filtered through a 0.45μm filter. Cells were plated in 6-well plates at a density of 300,000 cells/well and transduced with supernatants in the presence of 8 μg/mL Polybrene for 6 hours. Selection was carried out by treating the cells with 10 μg/ml Blasticidin for 5 days or 1 μg/ml Puromycin for 4 days. For siRNA transfections, 100,000 cells/well were plated in 6-well plates and transfected with 25nM of ON-TARGETplus MAFG siRNA pool

(Dharmacon, Cat # L-009109-00-0005) or Non-Targeting control (Cat # D-001810-10-05) using JetPrime (VWR, Cat # 89129-924) according to the manufacturer's protocol. 8 hours after transfection, cells were trypsinized and replated for cell biological assays.

Proliferation and colony formation assays

For proliferation assays, cells were plated in 96-well plates at a density of 1,000 - 2,500 cells/well and harvested for five days. Cells were fixed and stained with 0.1% crystal violet (VWR, Cat # 97061-850) solution in 20% methanol for 20 minutes followed by extraction of crystal violet with 10% acetic acid. Absorbance was measured at 600 nm using a plate reader. For colony formation assays, cells were plated in 6-well plates at a density of 1,000 - 2,000 cells/well and cultured for 2-3 weeks. Cells were fixed and stained with 0.1% crystal violet (VWR, Cat# 97061-850) solution in 20% methanol for 20 minutes. Colonies were quantified using Image J software.

Immunoblotting

Protein isolation was performed as previously described (Bok et al. 2019). 20μg of total protein were subjected to SDS-PAGE and Western blot, performed as previously described (Bok et al. 2019). Primary antibodies used were BRAF (Sigma, Cat # HPA001328), KRAS (Santa Cruz , Cat # sc-30), HA-Tag (Cell Signaling, Cat # 3724T), human p53 (Santa Cruz, Cat # sc-126), mouse p53 (BioVision, Cat # 3036-100), p21 (Abcam, Cat # ab109199), ERK (Cell Signaling, Cat # 4695), pERK (Cell Signaling Cat # 9101S), c-Jun (Cell Signaling Cat # 9165S), MAFG (Thermo Fisher Scientific, Cat # PA5-90907) and HSP90 (Cell Signaling, Cat # 4874)

ES cell targeting, mouse generation, and ESC-GEMM experiments

ES cell targeting and generation of chimeras was performed a described previously (Bok et al. 2019). Melanoma development was induced in 3-4 week old chimeras using 25mg/mL 4-OH Tamoxifen as described previously (Bok et al. 2019). Mice were fed 200mg/kg doxycycline (Envigo, Cat # TD180625) ad libitum. All animal experiments were conducted in accordance with an IACUC protocol approved by the University of South Florida. The derivation of the murine melanoma cell line from an ESC-GEMM chimera was performed as described previously (Bok et al. 2019).

Analysis of miR-29 target expression in The Cancer Genome Atlas

We obtained mRNA expression and survival data for KCTD5, MYBL2, SLC31A1, MAFG, RCC2, TUBB2A, SH3BP5L, SMS, and NCKAP5L of 354 skin cancer melanoma tumors from The Cancer Genome Atlas (TCGA). To generate a scoring for all nine genes with equal contribution, we normalized the mRNA expression values to the average for each gene, followed by calculating the average of each gene for each patient. For survival analysis, the data was stratified for patients with high or low score according to the median (cutoff: 0.96) and overall survival was estimated according to the Kaplan-Meier method. Groups were compared by the Log Rank test.

Statistical analysis

Statistical analysis was performed using GraphPad Prism software. Survival data were compared by applying the Log-rank (Mantel-Cox) test, and all other data were analyzed with the unpaired two-tailed t-test or ordinary one-way ANOVA. A p-value below 0.05 was considered statistically significant.

ACKNOWLEDGEMENTS

We thank A. Nyein and O. Balogun for technical assistance and Dr. I. Ibanez-de-Caceres for plasmids. This work was supported by grants to F.A.K. from the NIH/NCI (R03 CA227349) and the Melanoma Research Alliance (MRA Young Investigator Award and Team Science Award). This work was also supported by the Gene Targeting Core, Molecular Genomics Core, and Biostatistics and Bioinformatics Core, which are funded in part by Moffitt's Cancer Center Support Grant (NCI, P30-CA076292).

AUTHOR CONTRIBUTIONS

Conceptualization, FAK and OV; Methodology, FAK, OV, IB; Investigation, FAK, OV, IB, NJ, KN, XX and NM; Writing-Original Draft, FAK and OV; Writing – Reviewing and Editing, FAK, OV, IB, NJ, KN, XX and NM. Funding Acquisition, FAK; Resources, FAK; Supervision FAK.

REFERENCES

Alizadeh M, Safarzadeh A, Beyranvand F, Ahmadpour F, Hajiasgharzadeh K, Baghbanzadeh A, Baradaran B. 2019. The potential role of miR-29 in health and cancer diagnosis, prognosis, and therapy. *Journal of cellular physiology* **234**: 19280-19297.

Anders S, Pyl PT, Huber W. 2015. HTSeq--a Python framework to work with high-throughput sequencing data. *Bioinformatics* **31**: 166-169.

Ascierto PA, Kirkwood JM, Grob JJ, Simeone E, Grimaldi AM, Maio M, Palmieri G, Testori A, Marincola FM, Mozzillo N. 2012. The role of BRAF V600 mutation in melanoma. *Journal of translational medicine* **10**: 85.

Bates S, Phillips AC, Clark PA, Stott F, Peters G, Ludwig RL, Vousden KH. 1998. p14ARF links the tumour suppressors RB and p53. *Nature* **395**: 124-125.

Berger MF, Hodis E, Heffernan TP, Deribe YL, Lawrence MS, Protopopov A, Ivanova E, Watson IR, Nickerson E, Ghosh P et al. 2012. Melanoma genome sequencing reveals frequent PREX2 mutations. *Nature* **485**: 502-506.

Bok I, Vera O, Xu X, Jasani N, Nakamura K, Reff J, Nenci A, Gonzalez JG, Karreth FA. 2019. A versatile ES cell-based melanoma mouse modeling platform. *Cancer Res*.

Cancer Genome Atlas N. 2015. Genomic Classification of Cutaneous Melanoma. *Cell* **161**: 1681-1696.

Cloer EW, Goldfarb D, Schrank TP, Weissman BE, Major MB. 2019. NRF2 Activation in Cancer: From DNA to Protein. *Cancer Res* **79**: 889-898.

Cui H, Wang L, Gong P, Zhao C, Zhang S, Zhang K, Zhou R, Zhao Z, Fan H. 2015. Deregulation between miR-29b/c and DNMT3A is associated with epigenetic silencing of the CDH1 gene, affecting cell migration and invasion in gastric cancer. *PLoS One* **10**: e0123926.

Chang TC, Yu D, Lee YS, Wentzel EA, Arking DE, West KM, Dang CV, Thomas-Tikhonenko A, Mendell JT. 2008. Widespread microRNA repression by Myc contributes to tumorigenesis. *Nature genetics* **40**: 43-50.

Chen B, Wang J, Wang J, Wang H, Gu X, Tang L, Feng X. 2018. A regulatory circuitry comprising TP53, miR-29 family, and SETDB1 in non-small cell lung cancer. *Bioscience reports* **38**.

Davies H, Bignell GR, Cox C, Stephens P, Edkins S, Clegg S, Teague J, Woffendin H, Garnett MJ, Bottomley W et al. 2002. Mutations of the BRAF gene in human cancer. *Nature* **417**: 949-954.

Davis BN, Hata A. 2009. Regulation of MicroRNA Biogenesis: A miRiad of mechanisms. *Cell communication and signaling : CCS* **7**: 18.

Djebali S, Davis CA, Merkel A, Dobin A, Lassmann T, Mortazavi A, Tanzer A, Lagarde J, Lin W, Schlesinger F et al. 2012. Landscape of transcription in human cells. *Nature* **489**: 101-108.

Dobin A, Davis CA, Schlesinger F, Drenkow J, Zaleski C, Jha S, Batut P, Chaisson M, Gingeras TR. 2013. STAR: ultrafast universal RNA-seq aligner. *Bioinformatics* **29**: 15-21.

Fang M, Hutchinson L, Deng A, Green MR. 2016. Common BRAF(V600E)-directed pathway mediates widespread epigenetic silencing in colorectal cancer and melanoma. *Proc Natl Acad Sci U S A* **113**: 1250-1255.

Fattore L, Costantini S, Malpicci D, Ruggiero CF, Ascierto PA, Croce CM, Mancini R, Ciliberto G. 2017. MicroRNAs in melanoma development and resistance to target therapy. *Oncotarget* **8**: 22262-22278.

Freedberg DE, Rigas SH, Russak J, Gai W, Kaplow M, Osman I, Turner F, Randerson-Moor JA, Houghton A, Busam K et al. 2008. Frequent p16-independent inactivation of p14ARF in human melanoma. *Journal of the National Cancer Institute* **100**: 784-795.

Gray-Schopfer VC, Cheong SC, Chong H, Chow J, Moss T, Abdel-Malek ZA, Marais R, Wynford-Thomas D, Bennett DC. 2006. Cellular senescence in naevi and immortalisation in melanoma: a role for p16? *Br J Cancer* **95**: 496-505.

Gray-Schopfer VC, da Rocha Dias S, Marais R. 2005. The role of B-RAF in melanoma. *Cancer metastasis reviews* **24**: 165-183.

Hayes JD, Dinkova-Kostova AT. 2014. The Nrf2 regulatory network provides an interface between redox and intermediary metabolism. *Trends in biochemical sciences* **39**: 199-218.

Hewitt C, Lee Wu C, Evans G, Howell A, Elles RG, Jordan R, Sloan P, Read AP, Thakker N. 2002. Germline mutation of ARF in a melanoma kindred. *Hum Mol Genet* **11**: 1273-1279.

Hirotsu Y, Katsuoka F, Funayama R, Nagashima T, Nishida Y, Nakayama K, Engel JD, Yamamoto M. 2012. Nrf2-MafG heterodimers contribute globally to antioxidant and metabolic networks. *Nucleic Acids Res* **40**: 10228-10239.

Hodis E, Watson IR, Kryukov GV, Arold ST, Imielinski M, Theurillat JP, Nickerson E, Auclair D, Li L, Place C et al. 2012. A landscape of driver mutations in melanoma. *Cell* **150**: 251-263.

Hu Z, Klein JD, Mitch WE, Zhang L, Martinez I, Wang XH. 2014. MicroRNA-29 induces cellular senescence in aging muscle through multiple signaling pathways. *Aging* **6**: 160-175.

Hwang HW, Wentzel EA, Mendell JT. 2007. A hexanucleotide element directs microRNA nuclear import. *Science* **315**: 97-100.

Jackson EL, Willis N, Mercer K, Bronson RT, Crowley D, Montoya R, Jacks T, Tuveson DA. 2001. Analysis of lung tumor initiation and progression using conditional expression of oncogenic K-ras. *Genes Dev* **15**: 3243-3248.

Katsuoka F, Yamamoto M. 2016. Small Maf proteins (MafF, MafG, MafK): History, structure and function. *Gene* **586**: 197-205.

Ko T, Sharma R, Li S. 2019. Genome-wide screening identifies novel genes implicated in cellular sensitivity to BRAF(V600E) expression. *Oncogene*.

Kogure T, Costinean S, Yan I, Braconi C, Croce C, Patel T. 2012. Hepatic miR-29ab1 expression modulates chronic hepatic injury. *Journal of cellular and molecular medicine* **16**: 2647-2654.

Krauthammer M, Kong Y, Bacchiocchi A, Evans P, Pornputtapong N, Wu C, McCusker JP, Ma S, Cheng E, Straub R et al. 2015. Exome sequencing identifies recurrent mutations in NF1 and RASopathy genes in sun-exposed melanomas. *Nature genetics* **47**: 996-1002.

Krauthammer M, Kong Y, Ha BH, Evans P, Bacchiocchi A, McCusker JP, Cheng E, Davis MJ, Goh G, Choi M et al. 2012. Exome sequencing identifies recurrent somatic RAC1 mutations in melanoma. *Nature genetics* **44**: 1006-1014.

Kriegel AJ, Liu Y, Fang Y, Ding X, Liang M. 2012. The miR-29 family: genomics, cell biology, and relevance to renal and cardiovascular injury. *Physiological genomics* **44**: 237-244.

Kunz M, Loffler-Wirth H, Dannemann M, Willscher E, Doose G, Kelso J, Kottek T, Nickel B, Hopp L, Landsberg J et al. 2018. RNA-seq analysis identifies different

transcriptomic types and developmental trajectories of primary melanomas. *Oncogene* **37**: 6136-6151.
Kurinna S, Schafer M, Ostano P, Karouzakis E, Chiorino G, Bloch W, Bachmann A, Gay S, Garrod D, Lefort K et al. 2014. A novel Nrf2-miR-29-desmocollin-2 axis regulates desmosome function in keratinocytes. *Nat Commun* **5**: 5099.
Liu T, Yang H, Fan W, Tu J, Li TWH, Wang J, Shen H, Yang J, Xiong T, Steggerda J et al. 2018. Mechanisms of MAFG Dysregulation in Cholestatic Liver Injury and Development of Liver Cancer. *Gastroenterology* **155**: 557-571 e514.
Love MI, Huber W, Anders S. 2014. Moderated estimation of fold change and dispersion for RNA-seq data with DESeq2. *Genome Biology* **15**: 550.
Lloyd AC, Obermuller F, Staddon S, Barth CF, McMahon M, Land H. 1997. Cooperating oncogenes converge to regulate cyclin/cdk complexes. *Genes Dev* **11**: 663-677.
Martin M. 2011. Cutadapt removes adapter sequences from high-throughput sequencing reads. *2011* **17**: 3 %J EMBnet.journal.
Martinez I, Cazalla D, Almstead LL, Steitz JA, DiMaio D. 2011. miR-29 and miR-30 regulate B-Myb expression during cellular senescence. *Proc Natl Acad Sci U S A* **108**: 522-527.
Matsuo M, Nakada C, Tsukamoto Y, Noguchi T, Uchida T, Hijiya N, Matsuura K, Moriyama M. 2013. MiR-29c is downregulated in gastric carcinomas and regulates cell proliferation by targeting RCC2. *Mol Cancer* **12**: 15.
Michaloglou C, Vredeveld LC, Soengas MS, Denoyelle C, Kuilman T, van der Horst CM, Majoor DM, Shay JW, Mooi WJ, Peeper DS. 2005. BRAFE600-associated senescence-like cell cycle arrest of human naevi. *Nature* **436**: 720-724.
Mortazavi A, Williams BA, McCue K, Schaeffer L, Wold B. 2008. Mapping and quantifying mammalian transcriptomes by RNA-Seq. *Nat Methods* **5**: 621-628.
Mott JL, Kobayashi S, Bronk SF, Gores GJ. 2007. mir-29 regulates Mcl-1 protein expression and apoptosis. *Oncogene* **26**: 6133-6140.
Mott JL, Kurita S, Cazanave SC, Bronk SF, Werneburg NW, Fernandez-Zapico ME. 2010. Transcriptional suppression of mir-29b-1/mir-29a promoter by c-Myc, hedgehog, and NF-kappaB. *Journal of cellular biochemistry* **110**: 1155-1164.
Muthusamy V, Hobbs C, Nogueira C, Cordon-Cardo C, McKee PH, Chin L, Bosenberg MW. 2006. Amplification of CDK4 and MDM2 in malignant melanoma. *Genes, chromosomes & cancer* **45**: 447-454.
Nguyen T, Kuo C, Nicholl MB, Sim MS, Turner RR, Morton DL, Hoon DS. 2011. Downregulation of microRNA-29c is associated with hypermethylation of tumor-related genes and disease outcome in cutaneous melanoma. *Epigenetics* **6**: 388-394.
Nishikawa R, Chiyomaru T, Enokida H, Inoguchi S, Ishihara T, Matsushita R, Goto Y, Fukumoto I, Nakagawa M, Seki N. 2015. Tumour-suppressive microRNA-29s directly regulate LOXL2 expression and inhibit cancer cell migration and invasion in renal cell carcinoma. *FEBS letters* **589**: 2136-2145.
Peeper DS, Upton TM, Ladha MH, Neuman E, Zalvide J, Bernards R, DeCaprio JA, Ewen ME. 1997. Ras signalling linked to the cell-cycle machinery by the retinoblastoma protein. *Nature* **386**: 177-181.
Perna D, Karreth FA, Rust AG, Perez-Mancera PA, Rashid M, Iorio F, Alifrangis C, Arends MJ, Bosenberg MW, Bollag G et al. 2015. BRAF inhibitor resistance mediated by the AKT pathway in an oncogenic BRAF mouse melanoma model. *Proc Natl Acad Sci U S A* **112**: E536-545.

Ponting CP, Oliver PL, Reik W. 2009. Evolution and functions of long noncoding RNAs. *Cell* **136**: 629-641.

Romano G, Kwong LN. 2017. miRNAs, Melanoma and Microenvironment: An Intricate Network. *Int J Mol Sci* **18**.

Satyamoorthy K, Li G, Gerrero MR, Brose MS, Volpe P, Weber BL, Van Belle P, Elder DE, Herlyn M. 2003. Constitutive mitogen-activated protein kinase activation in melanoma is mediated by both BRAF mutations and autocrine growth factor stimulation. *Cancer Res* **63**: 756-759.

Shah NM, Zaitseva L, Bowles KM, MacEwan DJ, Rushworth SA. 2015. NRF2-driven miR-125B1 and miR-29B1 transcriptional regulation controls a novel anti-apoptotic miRNA regulatory network for AML survival. *Cell Death Differ* **22**: 654-664.

Sharpless NE, Kannan K, Xu J, Bosenberg MW, Chin L. 2003. Both products of the mouse Ink4a/Arf locus suppress melanoma formation in vivo. *Oncogene* **22**: 5055-5059.

Sherr CJ, Weber JD. 2000. The ARF/p53 pathway. *Current opinion in genetics & development* **10**: 94-99.

Sheu JJ, Guan B, Tsai FJ, Hsiao EY, Chen CM, Seruca R, Wang TL, Shih Ie M. 2012. Mutant BRAF induces DNA strand breaks, activates DNA damage response pathway, and up-regulates glucose transporter-1 in nontransformed epithelial cells. *The American journal of pathology* **180**: 1179-1188.

Sumimoto H, Imabayashi F, Iwata T, Kawakami Y. 2006. The BRAF-MAPK signaling pathway is essential for cancer-immune evasion in human melanoma cells. *The Journal of experimental medicine* **203**: 1651-1656.

Sun C, Zhang Z, Qie J, Wang Y, Qian J, Wang J, Wu J, Li Q, Bai C, Han B et al. 2018. Genetic polymorphism of SLC31A1 is associated with clinical outcomes of platinum-based chemotherapy in non-small-cell lung cancer patients through modulating microRNA-mediated regulation. *Oncotarget* **9**: 23860-23877.

Terzian T, Torchia EC, Dai D, Robinson SE, Murao K, Stiegmann RA, Gonzalez V, Boyle GM, Powell MB, Pollock PM et al. 2010. p53 prevents progression of nevi to melanoma predominantly through cell cycle regulation. *Pigment cell & melanoma research* **23**: 781-794.

Tuveson DA, Shaw AT, Willis NA, Silver DP, Jackson EL, Chang S, Mercer KL, Grochow R, Hock H, Crowley D et al. 2004. Endogenous oncogenic K-ras(G12D) stimulates proliferation and widespread neoplastic and developmental defects. *Cancer cell* **5**: 375-387.

Ugalde AP, Ramsay AJ, de la Rosa J, Varela I, Marino G, Cadinanos J, Lu J, Freije JM, Lopez-Otin C. 2011. Aging and chronic DNA damage response activate a regulatory pathway involving miR-29 and p53. *EMBO J* **30**: 2219-2232.

Vera O, Jimenez J, Pernia O, Rodriguez-Antolin C, Rodriguez C, Sanchez Cabo F, Soto J, Rosas R, Lopez-Magallon S, Esteban Rodriguez I et al. 2017. DNA Methylation of miR-7 is a Mechanism Involved in Platinum Response through MAFG Overexpression in Cancer Cells. *Theranostics* **7**: 4118-4134.

Viros A, Sanchez-Laorden B, Pedersen M, Furney SJ, Rae J, Hogan K, Ejiama S, Girotti MR, Cook M, Dhomen N et al. 2014. Ultraviolet radiation accelerates BRAF-driven melanomagenesis by targeting TP53. *Nature* **511**: 478-482.

Wei W, He HB, Zhang WY, Zhang HX, Bai JB, Liu HZ, Cao JH, Chang KC, Li XY, Zhao SH. 2013. miR-29 targets Akt3 to reduce proliferation and facilitate differentiation of myoblasts in skeletal muscle development. *Cell death & disease* **4**: e668.

Wozniak M, Mielczarek A, Czyz M. 2016. miRNAs in Melanoma: Tumor Suppressors and Oncogenes with Prognostic Potential. *Current medicinal chemistry* **23**: 3136-3153.

Wu GS. 2004. The functional interactions between the p53 and MAPK signaling pathways. *Cancer biology & therapy* **3**: 156-161.

Wu J, Rosenbaum E, Begum S, Westra WH. 2007. Distribution of BRAF T1799A(V600E) mutations across various types of benign nevi: implications for melanocytic tumorigenesis. *The American Journal of dermatopathology* **29**: 534-537.

Wu Z, Huang X, Huang X, Zou Q, Guo Y. 2013. The inhibitory role of Mir-29 in growth of breast cancer cells. *J Exp Clin Cancer Res* **32**: 98.

Xiong Y, Liu L, Qiu Y, Liu L. 2018. MicroRNA-29a Inhibits Growth, Migration and Invasion of Melanoma A375 Cells in Vitro by Directly Targeting BMI1. *Cellular physiology and biochemistry : international journal of experimental cellular physiology, biochemistry, and pharmacology* **50**: 385-397.

Yeh I, von Deimling A, Bastian BC. 2013. Clonal BRAF mutations in melanocytic nevi and initiating role of BRAF in melanocytic neoplasia. *Journal of the National Cancer Institute* **105**: 917-919.

Yu H, McDaid R, Lee J, Possik P, Li L, Kumar SM, Elder DE, Van Belle P, Gimotty P, Guerra M et al. 2009. The role of BRAF mutation and p53 inactivation during transformation of a subpopulation of primary human melanocytes. *The American journal of pathology* **174**: 2367-2377.

Yu PN, Yan MD, Lai HC, Huang RL, Chou YC, Lin WC, Yeh LT, Lin YW. 2014. Downregulation of miR-29 contributes to cisplatin resistance of ovarian cancer cells. *International journal of cancer* **134**: 542-551.

Zhang B, Ho YW, Huang Q, Maeda T, Lin A, Lee SU, Hair A, Holyoake TL, Huettner C, Bhatia R. 2012a. Altered microenvironmental regulation of leukemic and normal stem cells in chronic myelogenous leukemia. *Cancer cell* **21**: 577-592.

Zhang T, Dutton-Regester K, Brown KM, Hayward NK. 2016. The genomic landscape of cutaneous melanoma. *Pigment cell & melanoma research* **29**: 266-283.

Zhang X, Zhao X, Fiskus W, Lin J, Lwin T, Rao R, Zhang Y, Chan JC, Fu K, Marquez VE et al. 2012b. Coordinated silencing of MYC-mediated miR-29 by HDAC3 and EZH2 as a therapeutic target of histone modification in aggressive B-Cell lymphomas. *Cancer cell* **22**: 506-523.

Zhao JJ, Lin J, Lwin T, Yang H, Guo J, Kong W, Dessureault S, Moscinski LC, Rezania D, Dalton WS et al. 2010. microRNA expression profile and identification of miR-29 as a prognostic marker and pathogenetic factor by targeting CDK6 in mantle cell lymphoma. *Blood* **115**: 2630-2639.

FIGURE LEGENDS

Figure 1: Oncogenic BRAF and KRAS regulate miR-29 in MEFs. (A) Ectopic expression of $Braf^{V600E}$ or $Kras^{G12D}$ in wildtype MEFs elevates expression of p53 and pERK (Western blot, left panel) and mature miR-29a, miR-29b, and miR-29c (qRT-PCR, right panel). (B) Induction of $Braf^{V600E}$ expression by Adeno-Cre (Cre) in LSL- $Braf^{V600E}$ MEFs elevates expression of p53 and pERK (Western blot, left panel) and mature miR-29a, miR-29b, and miR-29c (qRT-PCR, right panel). MEFs infected with empty adenovirus (Mock) serve as controls. (C and D) qRT-PCRs showing the expression of pri-miR-29b1~a and pri-miR-29b2~c in wildtype MEFs following overexpression of $Braf^{V600E}$ or $Kras^{G12D}$ (C), and in LSL-$Braf^{V600E}$ MEFs following Adeno-Cre/Mock infection (D). * $p < 0.05$; *** $p < 0.001$; ns, not significant.

Figure 2: The MAPK pathway and p53 regulate miR-29 in MEFs. (A) qRT-PCRs showing the expression of pri-miR-29b1~a and pri-miR-29b2~c in wildtype MEFs following treatment with Doxorubicin or Mitomycin C. (B) Effect of p53 silencing on pri-miR-29b1~a and pri-miR-29b2~c expression measured by qRT-PCR in LSL-$Braf^{V600E}$ MEFs after induction of $Braf^{V600E}$ with Adeno-Cre. (C) Luciferase assay in shp53-expressing LSL-$Braf^{V600E}$ MEFs using a miR-29-Luciferase reporter. (D, E) Effect of MEK inhibitor (AZD6244) on the MAPK pathway and pri-miR-29b1~a and pri-miR-29b2~c expression in LSL-$Braf^{V600E}$ (D) and shp53-expressing LSL-$Braf^{V600E}$ MEFs (E). Western blots are shown in the left panels and expression of pri-miR-29b1~a and pri-miR-29b2~c measured by qRT-PCR are shown in the right panels of (B), (D) and (E). For all Western blots, Hsp90 was used as loading control. ns, not significant; * $p < 0.05$; ** $p < 0.01$; *** $p < 0.001$.

Figure 3: MAPK signaling and p53 regulate miR-29 in human melanocytes and melanoma. (A) Effect of Doxorubicin (Doxo) on pri-miR-29b1~a and pri-miR-29b2~c expression in human melanocytes Hermes1 (H1) and Hermes3A (H3). (B) Effect of TPA on pri-miR-29b1~a and pri-miR-29b2~c expression in human melanocytes. (C,D) Effect of AZD6244 on pri-miR-29b1~a and pri-miR-29b2~c expression in human melanocytes (C) and melanoma cells (D). (E) Expression of pri-miR-29b1~a and pri-miR-29b2~c in human melanocytes and melanoma cell lines obtained by RNAseq. (F) Expression of pri-miR-29b1~a and pri-miR-29b2~c in nevi and melanoma in the GSE112509 dataset. (G) Expression of pri-miR-29b1~a and pri-miR-29b2~c in parental Hermes1 and H1B cells obtained by RNAseq. (H) Effect of AZD6244 on pri-miR-29b1~a and pri-miR-29b2~c expression in H1B and H3B8 cells. pri-miR-29b1~a and pri-miR-29b2~c qRT-PCRs are shown in the left panels while Western blots are shown in the right panels of (A-D) and (H). For all western blots, HSP90 was used as loading control. ns, not significant; * $p < 0.05$; ** $p < 0.01$; *** $p < 0.001$; # FDR < 0.05; ## FDR < 0.01; ### FDR < 0.001.

Figure 4: miR-29 inactivation promotes melanoma progression. (A) Effect of miR-29 inactivation in A375 cells on colony formation by hairpin inhibitors. (B,C) Effect of miR-29 inactivation by a miR-29 sponge construct in A375 cells on proliferation (B) and colony formation (C). (D) Effect of the miR-29 sponge on miR-29-Luciferase reporter activity in A375 cells. (E) Outline of the embryonic stem cell-genetically engineered mouse model approach (Bok et al. 2019) where a Dox-inducible miR-29 sponge is expressed in $Braf^{V600E}$; $Pten^{\Delta/WT}$ melanocytes. (F, G) Kaplan-Meier curves comparing the tumor free survival (F) and overall survival (G) of $Braf^{V600E}$; $Pten^{\Delta/WT}$ GFP and miR-29 sponge chimeras.

Figure 5: miR-29 targets constitute a vulnerability of melanoma. (A) miR-29-Luciferase reporter activity in miR-29 sponge melanoma cells. Dox withdrawal turns off expression of the sponge construct resulting in miR-29 reactivation. (B, C) Proliferation (B) and colony formation (C) upon miR-29 reactivation in miR-29 sponge melanoma cells. (D) Correlation between pri-miR-29b2~c and MAFG in the GSE112509 dataset. (E) Expression of MAFG in 23 nevi and 57 melanomas obtained from the GSE112509 dataset. (F) Survival analysis from TCGA (PanCancer Atlas) comparing melanoma patients with high and low expression of the 9 putative miR-29 targets. * $p < 0.05$; ** $p < 0.01$; *** $p < 0.001$, # FDR < 0.05; ## FDR < 0.01; ### FDR < 0.001.

Figure 6: MAFG is directly regulated by miR-29. (A and B) MAFG mRNA (upper panels) and protein (lower panels) expression upon miR-29 inhibitors (left) or mimics (right) transfection in H1B (A) or WM164 (B). (C) Activity of MAFG 3'UTR Luciferase reporter in response to miR-29 inhibitors. (D) Activity of MAFG wildtype or miR-29 binding site-mutant 3'UTR Luciferase reporter in response to miR-29 mimics. (E) qRT-PCR showing the basal expression levels of MAFG mRNA in melanocytes and melanoma cells. (F) Western blot showing the basal expression levels of MAFG protein in melanocytes and melanoma cells. (G) Quantification of the Western blot shown in (F). (H) Western blot showing MAFG expression in response to TPA stimulation or $BRAF^{V600E}$ expression.

Figure 7: MAFG is a putative melanoma oncogene (A, B) The effect of MAFG overexpression in Hermes1 cells on proliferation (A) and colony formation (B). (C-F) Proliferation (C,E) and colony formation (D,F) of WM164 (C, D) or A375 (E, F) cells upon

MAFG silencing with a ON-TARGETplus MAFG siRNA pool. Western blots in (A, C and D) show the MAFG protein expression changes. For all Western blots, HSP90 was used as loading control. * $p < 0.05$; ** $p < 0.01$; *** $p < 0.001$.

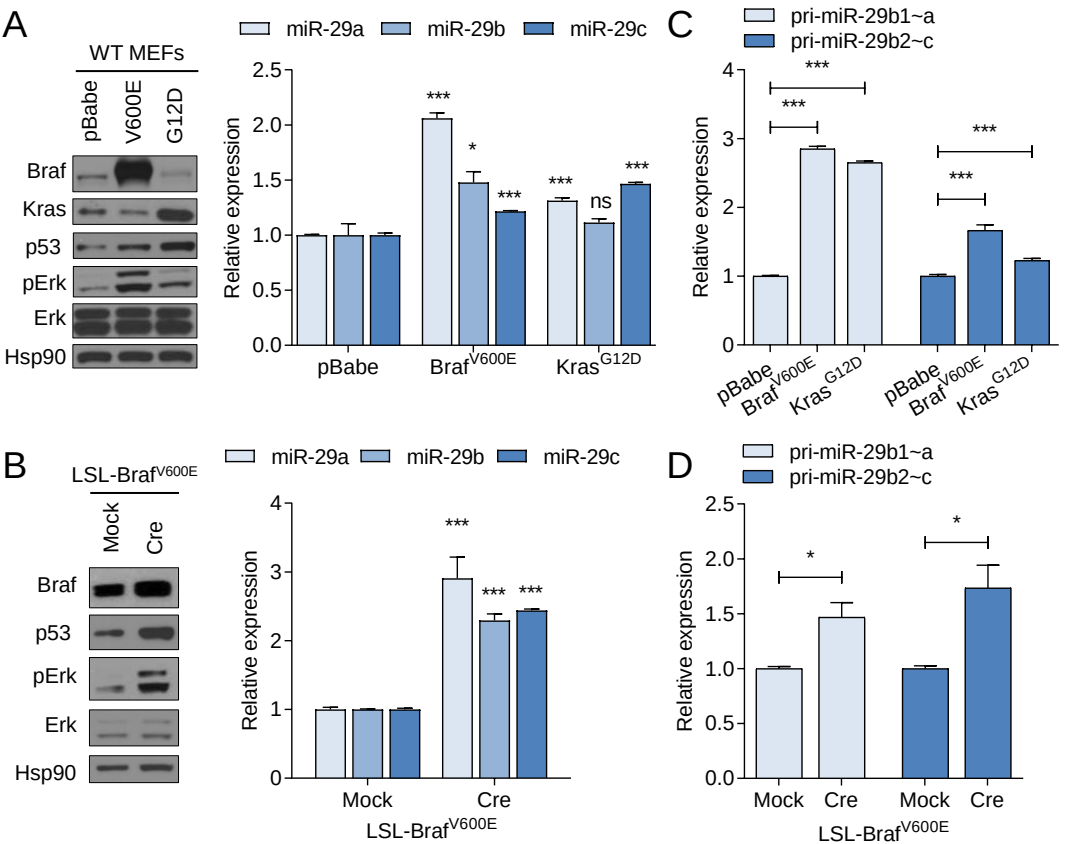
A
WT MEFs
pBabe
V600E
G12D
Braf
Kras
p53
pErk
Erk
Hsp90
miR-29a
miR-29b
miR-29c
Relative expression
2.5
2.0
1.5
1.0
0.5
0.0
***
*
***
***
ns
***
pBabe
Braf V600E
Kras G12D
C
pri-miR-29b1~a
pri-miR-29b2~c
4
3
2
1
0
***
***
***
***
pBabe
Braf V600E
Kras G12D
pBabe
Braf V600E
Kras G12D
B
LSL-Braf V600E
Mock
Cre
Braf
p53
pErk
Erk
Hsp90
miR-29a
miR-29b
miR-29c
Relative expression
4
3
2
1
0
***
***
***
Mock
Cre
LSL-Braf V600E
D
pri-miR-29b1~a
pri-miR-29b2~c
Relative expression
2.5
2.0
1.5
1.0
0.5
0.0
*
*
Mock
Cre
Mock
Cre
LSL-Braf V600E

Fig1

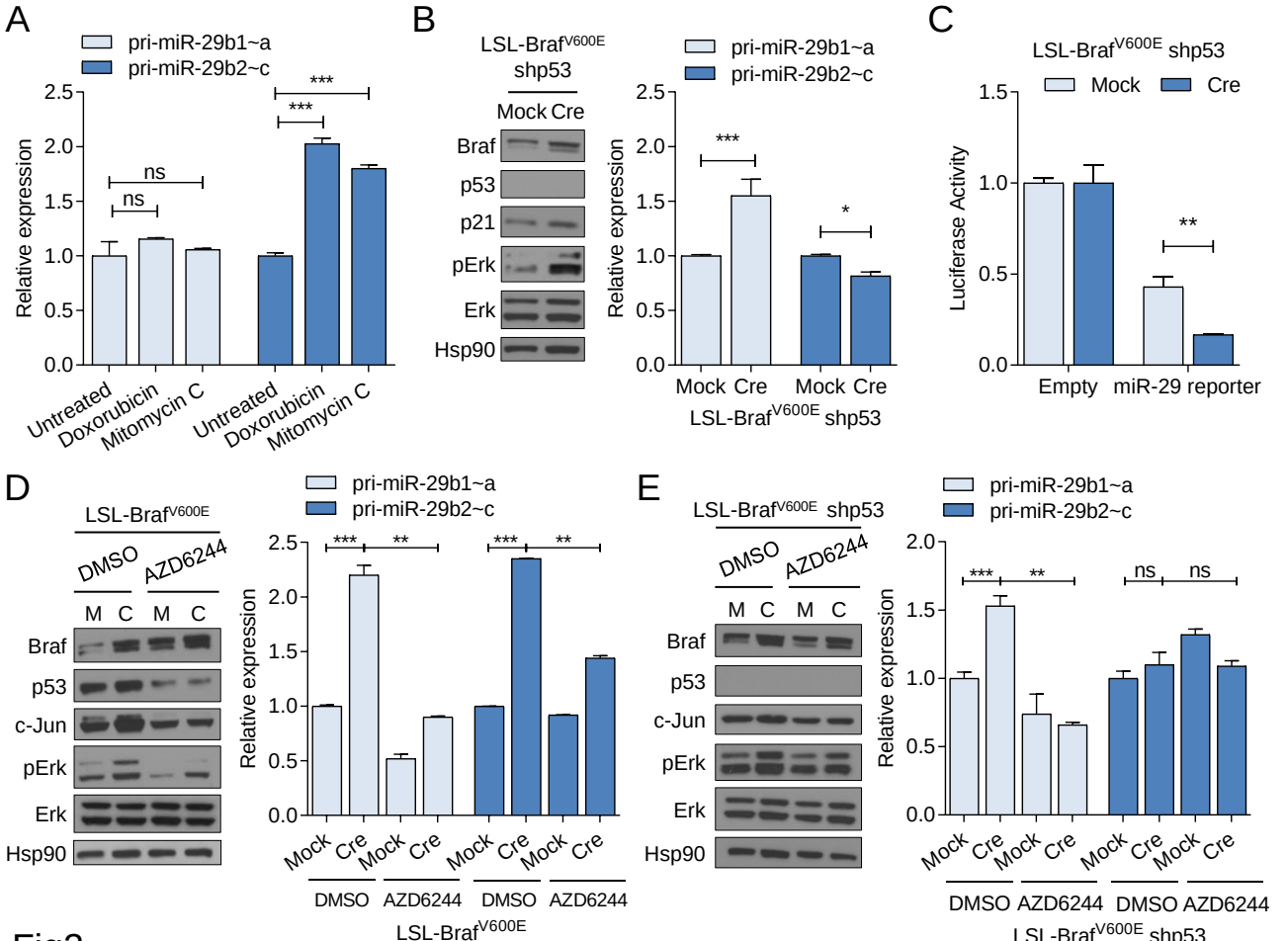
A
pri-miR-29b1~a
pri-miR-29b2~c
Relative expression
ns
ns
***
***
Untreated
Doxorubicin
Mitomycin C
Untreated
Doxorubicin
Mitomycin C
B
LSL-Braf^{V600E} shp53
Mock Cre
Braf
p53
p21
pErk
Erk
Hsp90
pri-miR-29b1~a
pri-miR-29b2~c
Relative expression
***
*
Mock Cre Mock Cre
LSL-Braf^{V600E} shp53
C
LSL-Braf^{V600E} shp53
Mock Cre
Luciferase Activity
**
Empty miR-29 reporter
D
LSL-Braf^{V600E}
DMSO AZD6244
M C M C
Braf
p53
c-Jun
pErk
Erk
Hsp90
pri-miR-29b1~a
pri-miR-29b2~c
Relative expression
***
**
***
**
Mock Cre Mock Cre Mock Cre Mock Cre
DMSO AZD6244 DMSO AZD6244
LSL-Braf^{V600E}
E
LSL-Braf^{V600E} shp53
DMSO AZD6244
M C M C
Braf
p53
c-Jun
pErk
Erk
Hsp90
pri-miR-29b1~a
pri-miR-29b2~c
Relative expression
***
**
ns
ns
Mock Cre Mock Cre Mock Cre Mock Cre
DMSO AZD6244 DMSO AZD6244
LSL-Braf^{V600E} shp53

Fig2

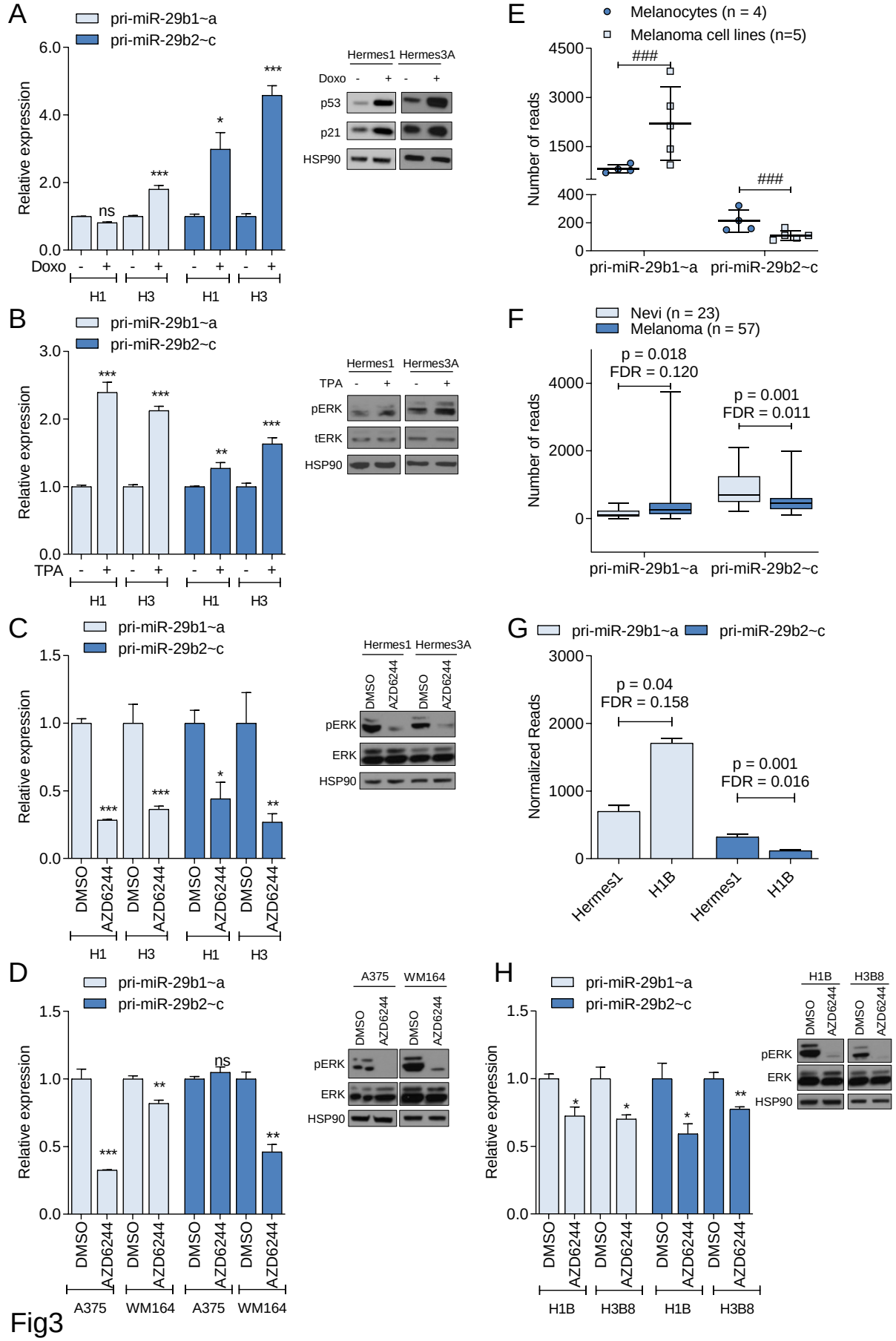
A
pri-miR-29b1~a
pri-miR-29b2~c
Relative expression
6.0
4.0
2.0
0.0
ns
***
*
***
Doxo - + - + - + - +
H1 H3 H1 H3
Hermes1 Hermes3A
Doxo - + - +
p53
p21
HSP90
B
pri-miR-29b1~a
pri-miR-29b2~c
Relative expression
3.0
2.0
1.0
0.0
***
***
**
***
TPA - + - + - + - +
H1 H3 H1 H3
Hermes1 Hermes3A
TPA - + - +
pERK
tERK
HSP90
C
pri-miR-29b1~a
pri-miR-29b2~c
Relative expression
1.5
1.0
0.5
0.0
***
***
*
**
DMSO AZD6244 DMSO AZD6244 DMSO AZD6244 DMSO AZD6244
H1 H3 H1 H3
Hermes1 Hermes3A
DMSO AZD6244 DMSO AZD6244
pERK
ERK
HSP90
D
pri-miR-29b1~a
pri-miR-29b2~c
Relative expression
1.5
1.0
0.5
0.0
***
**
ns
**
DMSO AZD6244 DMSO AZD6244 DMSO AZD6244 DMSO AZD6244
A375 WM164 A375 WM164
A375 WM164
DMSO AZD6244 DMSO AZD6244
pERK
ERK
HSP90
E
Melanocytes (n = 4)
Melanoma cell lines (n=5)
Number of reads
4500
3000
1500
400
200
0
###
###
pri-miR-29b1~a pri-miR-29b2~c
F
Nevi (n = 23)
Melanoma (n = 57)
Number of reads
4000
2000
0
p = 0.018
FDR = 0.120
p = 0.001
FDR = 0.011
pri-miR-29b1~a pri-miR-29b2~c
G
pri-miR-29b1~a pri-miR-29b2~c
Normalized Reads
3000
2000
1000
0
p = 0.04
FDR = 0.158
p = 0.001
FDR = 0.016
Hermes1 H1B Hermes1 H1B
H
pri-miR-29b1~a
pri-miR-29b2~c
Relative expression
1.5
1.0
0.5
0.0
*
*
*
**
DMSO AZD6244 DMSO AZD6244 DMSO AZD6244 DMSO AZD6244
H1B H3B8 H1B H3B8
H1B H3B8
DMSO AZD6244 DMSO AZD6244
pERK
ERK
HSP90

Fig3

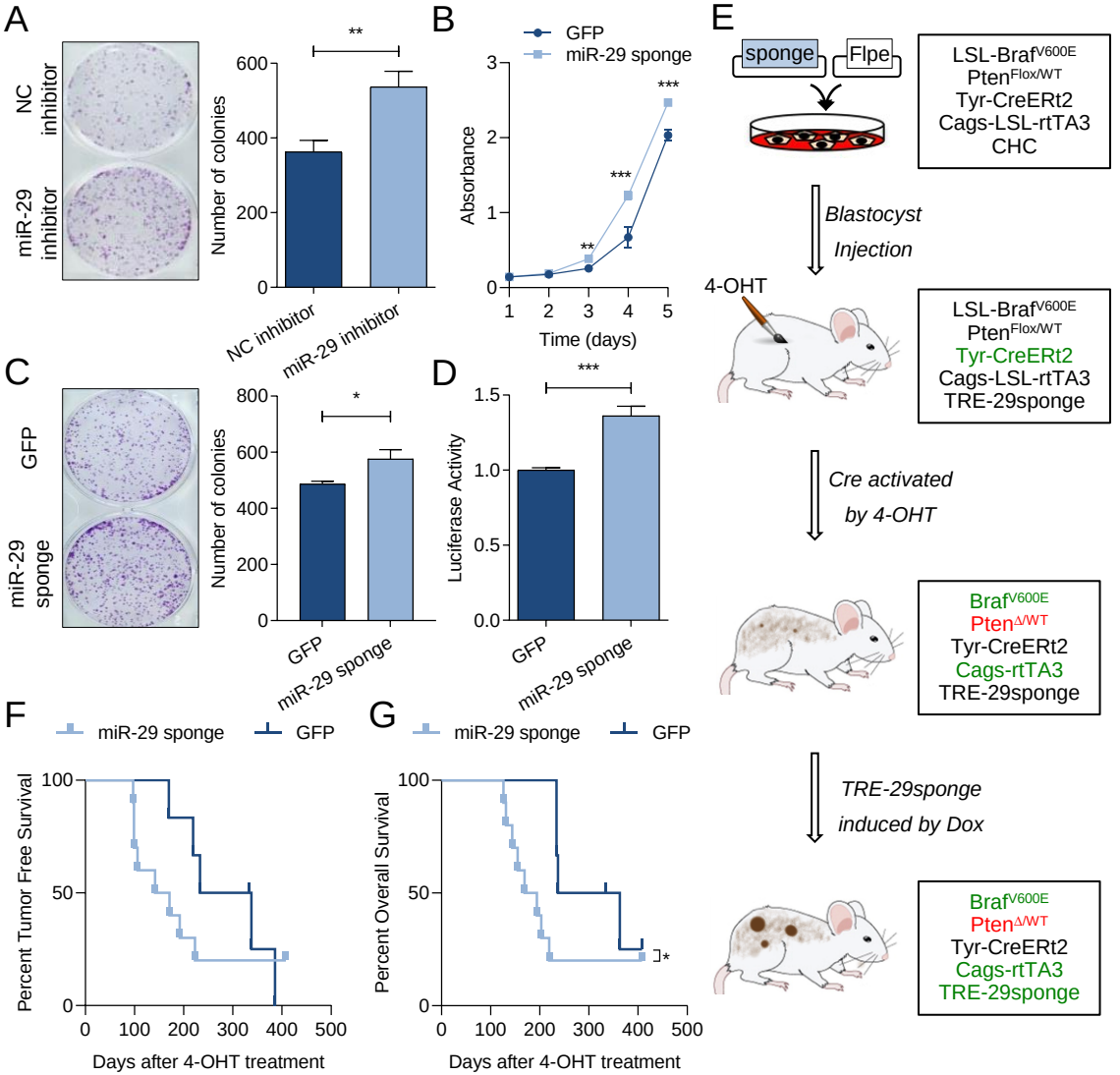
A
NC inhibitor
miR-29 inhibitor
Number of colonies
600
400
200
0
**
NC inhibitor
miR-29 inhibitor
B
GFP
miR-29 sponge
Absorbance
3
2
1
0
***
***
**
1
2
3
4
5
Time (days)
C
GFP
miR-29 sponge
Number of colonies
800
600
400
200
0
*
GFP
miR-29 sponge
D
Luciferase Activity
1.5
1.0
0.5
0.0
***
GFP
miR-29 sponge
E
sponge
Flpe
LSL-Braf V600E
Pten Flox/WT
Tyr-CreERt2
Cags-LSL-rtTA3
CHC
Blastocyst
Injection
4-OHT
LSL-Braf V600E
Pten Flox/WT
Tyr-CreERt2
Cags-LSL-rtTA3
TRE-29sponge
Cre activated
by 4-OHT
Braf V600E
Pten Δ/WT
Tyr-CreERt2
Cags-rtTA3
TRE-29sponge
TRE-29sponge
induced by Dox
Braf V600E
Pten Δ/WT
Tyr-CreERt2
Cags-rtTA3
TRE-29sponge
F
miR-29 sponge
GFP
Percent Tumor Free Survival
100
50
0
0
100
200
300
400
500
Days after 4-OHT treatment
G
miR-29 sponge
GFP
Percent Overall Survival
100
50
0
*
0
100
200
300
400
500
Days after 4-OHT treatment

Fig4

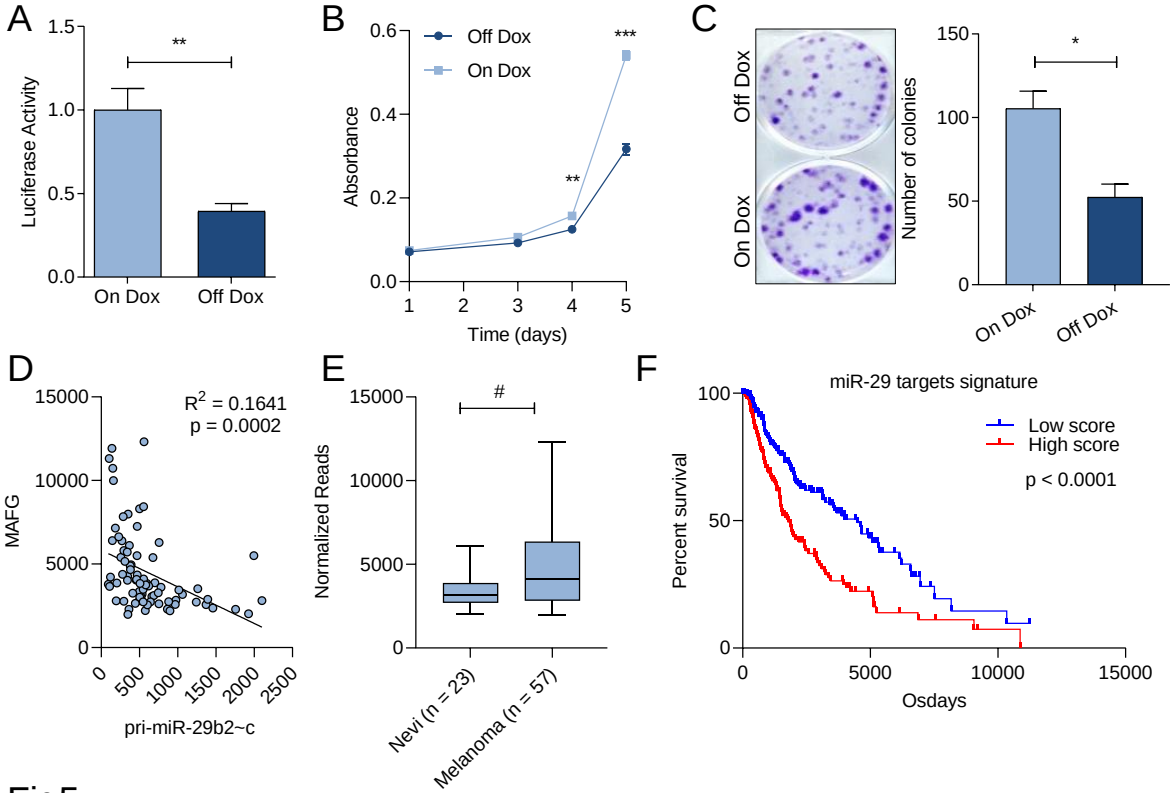
A
Luciferase Activity
1.5
1.0
0.5
0.0
**
On Dox
Off Dox
B
Absorbance
0.6
0.4
0.2
0.0
Off Dox
On Dox
***
**
1
2
3
4
5
Time (days)
C
Off Dox
On Dox
Number of colonies
150
100
50
0
*
On Dox
Off Dox
D
MAFG
15000
10000
5000
0
R2 = 0.1641
p = 0.0002
0
500
1000
1500
2000
2500
pri-miR-29b2~c
E
Normalized Reads
15000
10000
5000
0
#
Nevi (n = 23)
Melanoma (n = 57)
F
miR-29 targets signature
Percent survival
100
50
0
Low score
High score
p < 0.0001
0
5000
10000
15000
Osdays

Fig5

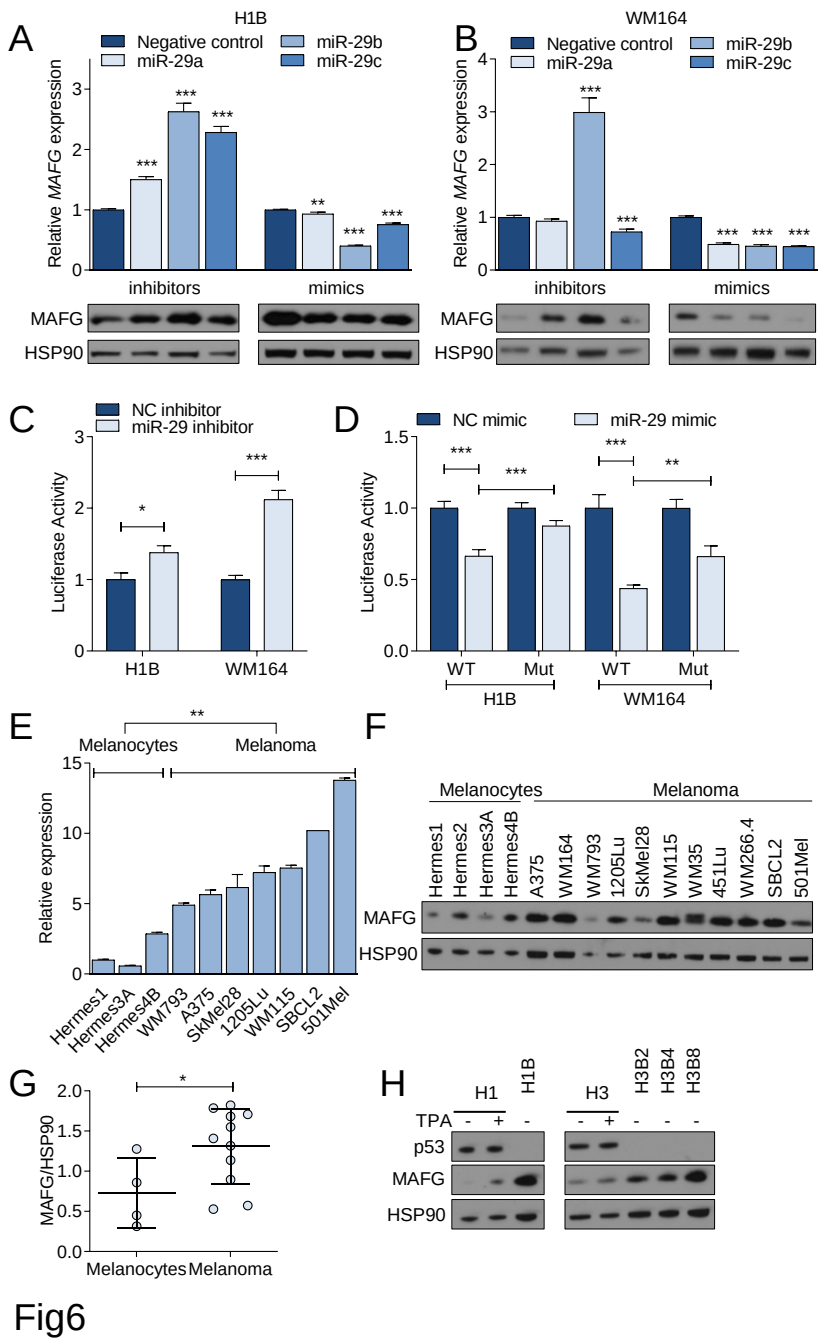
A
H1B
Negative control
miR-29a
miR-29b
miR-29c
Relative MAFG expression
inhibitors
mimics
MAFG
HSP90
B
WM164
C
NC inhibitor
miR-29 inhibitor
Luciferase Activity
H1B
WM164
D
NC mimic
miR-29 mimic
WT
Mut
E
Melanocytes
Melanoma
Relative expression
Hermes1
Hermes3A
Hermes4B
WM793
A375
SkMel28
1205Lu
WM115
SBCL2
501Mel
F
Hermes2
WM164
WM35
451Lu
WM266.4
G
MAFG/HSP90
H
H1
H1B
H3
H3B2
H3B4
H3B8
TPA
p53

Fig6

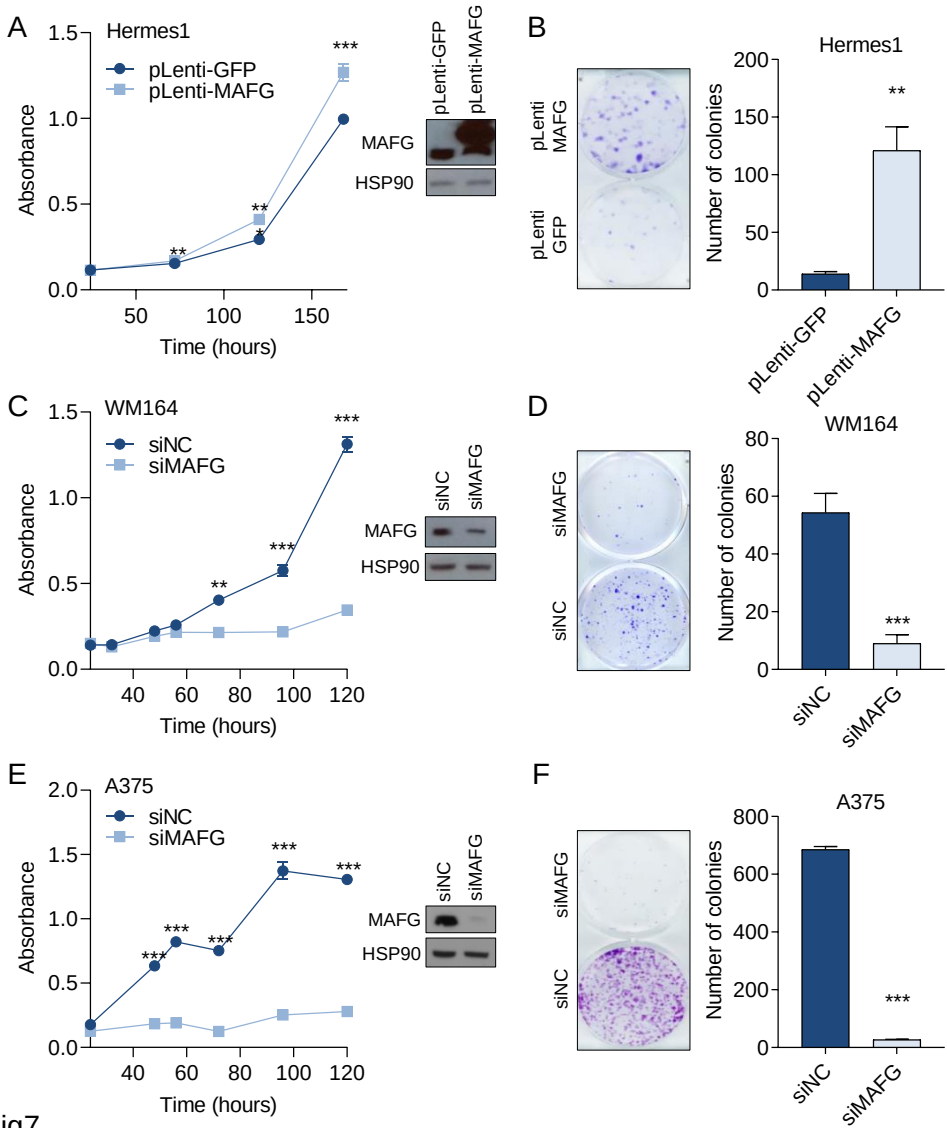
A
Hermes1
pLenti-GFP
pLenti-MAFG
Absorbance
Time (hours)
pLenti-GFP
pLenti-MAFG
MAFG
HSP90
B
Hermes1
pLenti MAFG
pLenti GFP
Number of colonies
pLenti-GFP
pLenti-MAFG
C
WM164
siNC
siMAFG
Absorbance
Time (hours)
siNC
siMAFG
MAFG
HSP90
D
WM164
siMAFG
siNC
Number of colonies
siNC
siMAFG
E
A375
siNC
siMAFG
Absorbance
Time (hours)
siNC
siMAFG
MAFG
HSP90
F
A375
siMAFG
siNC
Number of colonies
siNC
siMAFG

Fig7